

Review

Carbon Materials as Cathode Constituents for Electrochemical CO₂ Reduction—A Review

Sofia Messias, Manuel Nunes da Ponte  and Ana S. Reis-Machado * 

LAQV, REQUIMTE, Departamento de Química, Faculdade de Ciências e Tecnologia, Universidade Nova de Lisboa, Campus de Caparica, 2829-516 Caparica, Portugal; s.messias@campus.fct.unl.pt (S.M.); mnponce@fct.unl.pt (M.N.d.P.)

* Correspondence: ams.machado@fct.unl.pt; Tel.: +351 212948300

Received: 2 October 2019; Accepted: 5 December 2019; Published: 11 December 2019



Abstract: This work reviews the latest developments of cathodes for electrochemical CO₂ reduction, with carbon black, mesoporous carbons, carbon nanofibers, graphene, its derivatives and/or carbon nanotubes as constituents. Electrochemical CO₂ reduction into fuels and chemicals powered by renewable energy is a technology that can contribute to climate change mitigation. Strategies used in this fast-evolving field are discussed, having in mind a commercial application. Electrochemical performance of several materials is analyzed, using in some cases the findings of theoretical computational studies, which show the enormous potential of these materials. Considerable challenges still lie ahead to bring this technology into industrial deployment. However, the significant progress achieved so far shows that further R&D efforts might pay off.

Keywords: electrochemical reduction of CO₂; electro-catalysis; nanocarbon catalysts; carbon nanotubes; graphene; CO₂ utilization

1. Introduction

In the 1980s, carbon science was considered a mature discipline. This situation drastically changed in 1985 with the synthesis of the first molecule containing only carbon, buckminsterfullerene [1]. Later, Iijima's work in 1991 triggered an enormous interest in other novel carbon architectures structurally related to fullerene, namely carbon nanofibers and nanotubes [2]. This interest spread to many fields of science, due to the high potential of these materials for use in many applications. One of these specific applications is in CO₂ electrochemical reduction (CO₂ER). This is a promising technology in research phase for large-scale carbon management applications, because it can convert captured CO₂ into fuels or chemicals using renewable energy. CO₂ utilization technologies have the potential to reduce annual greenhouse gas emissions by up to 3.5 Gt CO₂-eq in 2030 [3]. Thus, they are able to contribute to climate change mitigation.

In order to be commercially deployed, CO₂ER must exhibit high production rates (current densities), high selectivity (faradaic efficiencies for the desired products), high energy efficiencies (low overpotentials) and stable performances. It has been challenging to achieve these conditions simultaneously. Due to the stability of the CO₂ molecule, its electro-reduction is a sluggish reaction, requiring high overpotentials and plagued with stability issues.

Carbon materials have been one of the materials of choice as constituents of electrodes for CO₂ electro-reduction, and although depending on their fabrication process, they can be classified as sustainable materials. They have been used according to several strategies to improve CO₂ER. This work reviews the latest developments of cathodes for CO₂ER, with carbon black, mesoporous carbons, carbon nanofibers, graphene and its derivatives and/or carbon nanotubes as constituents. Methods of cathode assembly are also referred to. The strategies used in this fast-evolving field are discussed, having in mind a commercial application. Electrochemical performances of several materials,

considering the findings of theoretical computational studies, are in some cases analyzed, when this type of study is available. Knowledge gaps and new promising R&D trends of nanocarbon-based materials development for this application are highlighted.

2. Carbon Black

Carbon black is produced by the incomplete combustion of petroleum heavy fractions. It is a form of para-crystalline carbon of high surface area. Although activated carbon has a more favorable surface area to volume ratio ($>1000 \text{ m}^2/\text{g}$) than carbon black, its low electrical conductivity makes it unsuitable as electrode material. Commercial carbon blacks, such as Vulcan or Ketjen black have been most frequently used as support to ensure large electrochemical reaction surfaces and to reduce noble metal loading.

2.1. Metal and Metal-Derived Particles Supported on Carbon Black

CO_2ER can be carried out in gas phase, where gaseous CO_2 is fed to the cathode through gas diffusion electrodes (GDE), or in liquid phase, where CO_2 dissolved in the liquid electrolyte contacts the electrode. Figure 1 presents a schematic diagram of two possible configurations of both operation modes.

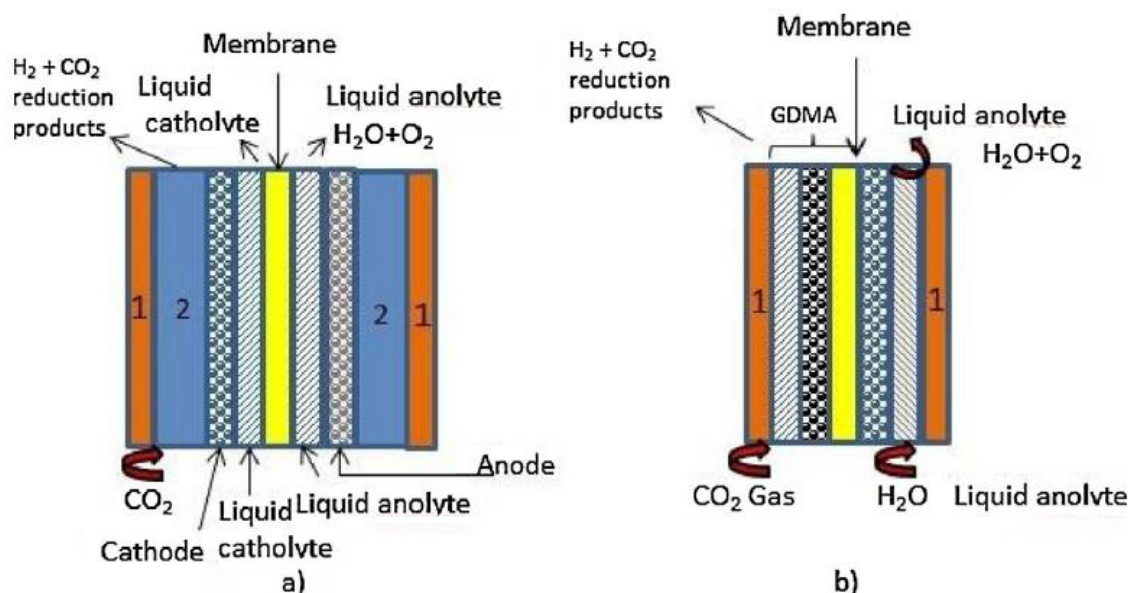


Figure 1. (a) Liquid-phase electrochemical reduction; (b) gas-phase electrochemical reduction. (1) Current collector, (2) gas diffusion layer, GDMA—gas diffusion membrane electrode layer assembly. Reproduced with permission from [4]. Copyright, Elsevier B. V., 2017.

In the liquid phase cell, the availability of CO_2 to react on the surface of the electrode is limited by the solubility of CO_2 in the electrolyte. At room temperature and pressure the solubility of CO_2 in water is only 33 mM [5]. To circumvent this problem, the use of GDEs was proposed [6]. In fact, one of the first uses of carbon materials in electrochemical reduction of CO_2 was as support for metal-based catalysts in gas-phase CO_2 electro-reduction [7]. Leveraging the knowledge acquired with GDEs in fuel cells [8], GDEs for electro-reduction of CO_2 were implemented and investigated. These type of electrodes usually consist of Teflon bonded catalyst particles and carbon black forming a catalyst ink that is pressed or fabricated over the cathode substrate. This substrate can itself be a carbon material, as for instance glassy carbon, carbon paper, carbon cloth, or another type of electric conducting material, for instance a metallic mesh. The catalyst inks can be applied on the substrate using several methods, such as brushing, rolling, or dipping, forming the catalyst layer [7]. This layer together with a gas diffusion layer (porous material that can also be made of carbon) and with the membrane constitute

the gas diffusion membrane electrode assembly (GDMA). Figure 2 shows a schematic representation of a gas-phase set-up indicating the localization of the GDE electrode and its components.

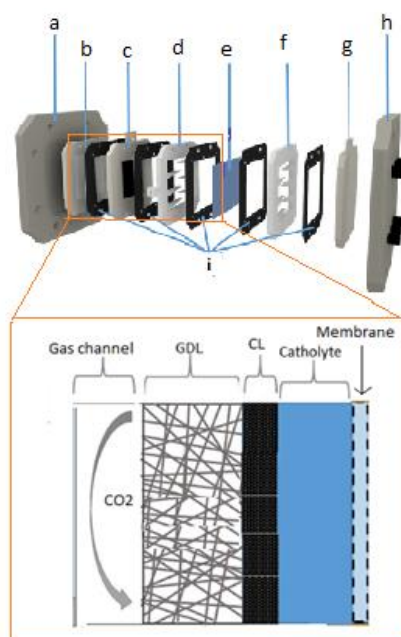


Figure 2. Schematic representation of the gas-phase set-up. (a) Back plate; (b) gas flow channel; (c) cathode GDE; (d) catholyte flow channel; (e) membrane; (f) anolyte flow channel; (g) anode; (h) front plate; (i) gaskets; GDL—gas diffusion layer; CL—catalytic layer. Modified and reproduced with permission from [9]. Copyright Elsevier B. V., 2019.

The following pioneer work was carried out employing GDEs with metal catalyst particles supported on carbon black, at ambient temperature and pressure. Mahmood et al. used Pb, In and Sn particles supported on Vulcan 72 [6]. CO_2 was reduced to HCOOH on Pb GDEs in aqueous acidic electrolyte with faradaic efficiencies in excess of 80%. At an applied current density of 115 mA cm^{-2} (pH 2), the potential of the cathode rose from -2.7 V to -3.0 V vs. SCE. The equivalent ohmic drop (IR drop) corrected cathode potentials were -1.5 V rising to -1.8 V vs. SCE. In and Sn showed lower catalytic activity. When Ru-Pd alloy particles were employed as the catalyst, HCOOH was obtained at a current density of 80 mA cm^{-2} and an applied potential of -1.1 V vs. SHE, in a 0.5 M KHCO_3 electrolyte [10]. Cook et al. carried out electrolysis with copper particles supported on carbon black, in KOH electrolyte solution with the current yield of 53% for C_2H_4 formation at -4.75 V vs. Ag/AgCl (including IR drop) and obtained a current density of 667 mA cm^{-2} [11]. Ikeda et al. obtained a current density of 300 mA cm^{-2} at -1.25 V vs. SHE. Ethylene and ethanol were the main products detected [7].

In an interesting work, gas-diffusion electrodes of various metal catalysts supported on carbon black (Cr, Mo, Mn, Ru, Co, Rh, Ir, Ni, Pd, Pt, Cu, Ag, Au, Zn, Cd, In, Ti, Sn, and Pb) were used to reduce CO_2 and nitrite ions dissolved in the electrolyte simultaneously [12]. The aqueous electrolyte consisted of 0.2 M KHCO_3 and 0.02 M KNO_2 .

Urea was one of the reaction products. It resulted from the reaction of the ammonia-like precursor formed from the reduction of nitrite ions, and the CO-like precursor formed from CO_2 electro-reduction in the presence of metal catalysts from the groups 11–14.

Near the turn of the century, the first works investigating CO_2 electro-reduction at high pressure on GDE electrodes were undertaken [13,14]. A GDE loaded with Pt catalyst supported on carbon black reduced CO_2 into methane at 20 bar with a faradaic efficiency of 38.8% with a very high partial current density of 600 mA cm^{-2} at an applied potential corrected for the IR drop of -1.93 V vs. Ag/AgCl. The electrolyte used was 0.5 M KHCO_3 . Ethylene, ethanol, ethane, carbon monoxide and formic acid were also produced [15]. Despite pressure being a very significant process intensification parameter,

the studies of the influence of pressure stopped from the late nineties of the last century [4] until 2004 with one paper published [16]. These studies were only resumed in 2012 with the work of Dufeck et al. [17]. Despite the impressive increase in current density achieved by the several GDE cathodes and the variety of different catalysts investigated supported on carbon black, all these works have in common the very high overpotential necessary to carry out CO₂ reduction both at atmospheric and at high pressure. Consequently, these processes present low energy efficiencies, with the exception of the aforementioned work of Dufeck et al., who achieved a significant increase in energy efficiency of the process (50%).

Further studies were conducted, in which catalyst particles with controlled particle size were dispersed onto carbon black. In particular, recent advances in the synthesis of nanoparticles (NP) allowed the examination of the potential for increasing reaction kinetics, due to the possibility of controlling surface area and surface morphologies. The effect of controlling the surface area by the use of nanoparticles, without the additional effect of dispersing the nanoparticles on a high surface area support, such as carbon black, is clearly illustrated by the work of Manthiram et al. [18]. In this work, Cu NP loaded on glassy carbon presented a faradaic efficiency up to ca. 80% for CH₄ generation, with four times higher energy efficiency than the one obtained with a Cu foil cathode.

It is current knowledge that nanoparticle size and shape influence CO₂ electro-reduction. For example, Zhu et al. [19] showed that an ink containing 8 nm Au NP monodispersed on Ketjen black and painted directly onto the carbon paper support presented the maximum faradaic efficiency for CO up to 90% at -0.67 V vs. RHE with a mass activity of 3 A g^{-1} in 0.5 M KHCO_3 electrolyte. When 500 nm long Au nanowires were used, at an applied potential of -0.35 V vs. RHE, the reduction faradaic efficiency (FE) reached 94% with a current density of 8.16 mA cm^{-2} (mass activity $1.84\text{ A g}^{-1}\text{ Au}$) [20].

Cathodes based on Au₂₅ clusters dispersed on Vulcan XC-72R carbon black catalyst ink deposited on glassy carbon promoted the CO₂ to CO reaction exhibiting an approximate 200–300 mV improvement over larger Au nanoparticles and bulk Au. Peak CO₂ conversion occurred at -1 V vs. RHE with approximately 100% efficiency and a rate 7–700 times higher than that for larger Au catalysts. Productivities for CO formation of $1.26\text{ mmol cm}^{-2}\text{ h}^{-1}$ were obtained in 0.1 M KHCO_3 electrolyte [21]. The reversible Au₂₅–CO₂ interaction was explained by density functional theory (DFT) using a CO₂-induced redistribution of charge within the cluster. Triangular Ag nanoplates were shown to reduce CO₂ to CO with an FE of 96.8% in 0.5 M KHCO_3 at -0.86 V vs. RHE, demonstrating that the edge site of Ag is the site responsible for CO selectivity [22].

Anchoring metal nanoparticles on carbon surface is another strategy to minimize agglomeration and for enhancing interfacial contact, promoting catalytic activity. Kim et al. [23] anchored Ag nanoparticles on carbon black with cysteamine and observed a decrease of the overpotential by 300 mV at 1 mA cm^{-2} , and four-fold enhanced CO faradaic efficiency at -0.75 V vs. RHE with the optimal particle size of 5 nm compared to polycrystalline Ag foil.

A further strategy consists of regulating NP catalyst selectivity for CO₂ER via the preparation of tunable core/shell structures. Li et al. [24] prepared Ketjen black inks containing SnO₂ coated over Cu nanoparticles. They found out that reduction becomes Sn-thickness dependent. The thicker (1.8 nm) shell showed Sn-like activity to generate formate while the thinner (0.8 nm) shell was selective to the formation of CO. A current density of 4.6 mA cm^{-2} , faradaic efficiency of 93% were reported at -0.7 V vs. RHE in liquid phase electrolysis employing 0.5 M KHCO_3 as electrolyte.

Polycrystalline Pd is recognized as a poor CO₂ reduction catalyst. It yields CO as major product. Current densities of 5 mA cm^{-2} with 10–30% Faraday efficiency (FE) for CO and 0–3% FE for HCO₂[−] at -0.8 to -1.0 V vs. RHE in aqueous bicarbonate solutions were obtained [25–28]. Dispersing Pd nanoparticles of ca. 5 nm on carbon black Vulcan XC-72 support allowed the selectivity towards formate to be changed [29]. In liquid phase electrolysis high mass activities 50–80 mA per mg of Pd (current densities of 2.2 to 4.15 mA cm^{-2} with FE > 95% after 3 h) for HCO₂[−] formation were obtained when driven by less than 200 mV of overpotential in aqueous bicarbonate solutions. The change in selectivity and increase in activity is attributed to a different reduction mechanism. On most materials

the reduction proceeds via electron transfer to CO_2 , which requires a high overpotential. On Pd the rate-determining step was found to be the addition of electrochemically generated surface adsorbed hydrogen to CO_2 . Furthermore, as Pd/C has a high surface area to mass ratio, when compared to Pd foil, H adsorption is enhanced resulting in increased formate production.

The work of Del Castillo et al. [30] represents a step forward in the few studies of CO_2 ER to formate in continuous mode. A GDE was prepared by air-brushing an ink containing Sn NP supported on carbon black (Vulcan) onto the gas diffusion layer. This component consisted of a Vulcan microporous layer with a binder that was also brushed onto carbon paper. Gas-phase electrolyses were carried out. The catholyte was a $0.45 \text{ mol L}^{-1} \text{ KHCO}_3 + 0.5 \text{ mol L}^{-1} \text{ KCl}$ aqueous solution and the anolyte was a $1 \text{ mol L}^{-1} \text{ KOH}$ aqueous solution with an anolyte flow per electrode area (Q/A ratio) of $0.57 \text{ mL min}^{-1} \text{ cm}^{-2}$. Pure gaseous CO_2 was fed to the cell at a flow of 200 mL min^{-1} . The catholyte and the anolyte only passed once through the cell. At a current density of 150 mA cm^{-2} it was possible to achieve a formate concentration of 2.5 g L^{-1} with a FE of 70%. At the expense of lowering FE, at current density of 200 mA cm^{-2} , cell voltage of ca. -4 V and employing a lower flow rate, it was possible to obtain formate concentrations up to 16 g L^{-1} .

Recently, nickel nitride was reported as another promising metal-like catalyst for generating CO. This material acted as CO_2 surface enrichment material. The catalysts consisted of nickel nitride supported on Vulcan carbon black yielded a current density of 23.3 mA cm^{-2} , faradaic efficiency for CO of 92.5% at -0.90 V vs. RHE with a cell voltage of 2.8 V [31].

A further interesting strategy involved the incorporation in anionic membranes of the ability of imidazolium ionic liquids to catalyze CO_2 reduction [32]. This was achieved by functionalizing a solid membrane with a styrene backbone with 1-methyl imidazole. Using an Ag GDE electrode without a porous carbon as constituent of the catalyst ink, sprayed onto a carbon gas diffusion layer and these novel membranes, it was possible to raise the current at 3 V cell voltage by a factor of 14 in gas-phase electrolyses. Current densities higher than 100 mA/cm^2 at 3 V voltages with CO product selectivity over 98% were obtained. Further improved performance was obtained by incorporating an anion exchange ionomer and carbon black into the Ag cathode. Potentiometric electrolysis in gas phase at a fixed current of 200 mA cm^{-2} showed that 98% selectivity could be maintained at about 3 V voltage for five months, with a voltage increase of only $3 \mu\text{V/hour}$. The improved performance was attributed to the extended three phase boundaries in Ag cathode [33]. These orders of magnitude of current densities are already meaningful for industrial deployment.

2.2. Molecular Catalysts

Another promising strategy that has been investigated is the integration of metal complexes with carbon materials, establishing the link between heterogeneous and homogeneous catalysis. These metal complexes are composed of metal centers with tunable oxidation states and macrocyclic organic ligands providing chemical stability and storage of reducing intermediates and/or protons.

Several organic-metallic compounds have been studied as molecular homogeneous catalysts for CO_2 ER. This type of work has been reviewed by Qiao et al. [34]. Thus, their catalytic activity and selectivity towards CO_2 ER is already known for many of them. However, when the goal is to get these molecules to work as CO_2 ER heterogeneous catalysts, linked to a support, this task is often very challenging. The difficulties are assuring the stability of the molecular catalysts after a high number of cycles and the need for a cost-effective method to separate the catalyst from the electrolyte.

Phthalocyanines and porphyrin metal complexes have been most studied for several decades but still present challenges in terms of productivities, energy efficiencies and stability.

GDEs of Co-, Mn-, Zn-, Cu phthalocyanines were examined as catalysts for CO_2 electro-reduction. Co-Pc showed the best performance yielding near 100% selectivity for CO at 80 mA cm^{-2} and -4.39 V vs. Ag/AgCl applied potential in aqueous electrolyte consisting of solutions of H_2SO_4 , phosphate or borate buffers with ionic strength of 3 ensured by Na_2SO_4 [35]. When electrolyses were conducted in dilute H_2SO_4 solutions (pH 2), current densities of 137 mA/cm^2 and faradaic efficiencies for CO of 14%

were obtained at -2.2 V vs. SCE applied potential. At an applied potential of -1.5 V vs. SCE current densities of 22 mA cm^{-2} and faradaic efficiencies for CO of 100% were observed [36].

The coupling of CO_2ER with nitrite ions reduction was also investigated, where the metal catalysts were replaced by metallophthalocyanines (M-Pc) [37,38]. The formation of urea, CO, formic acid and ammonia at the gas-diffusion electrodes with group 8–14 catalysts, except for Al and Ge, was observed. The maximum current efficiency of urea formation was about 40% at -1.5 V vs. SHE on Ni-Pc catalysts. The ability for urea formation on various M-Pc catalysts depends on the current efficiencies of both CO and NH_3 formation.

Recently, Wang et al. designed a Co phthalocyanine (CoPc2) bearing one trimethyl ammonium moiety and three tert-butyl groups appended on the phthalocyanine macrocycle [39]. Figure 3 shows the formula of this complex and presents current density, selectivity for CO production as a function of the potential and the bulk electrolysis curve at fixed potential ($E = -0.72$ V vs. RHE), illustrating the performance of one of the best catalytic systems using state-of-the-art molecular catalysts. The complex was dispersed into porous films of carbon black powder or multiwalled carbon nanotubes. Electrolysis in gas phase was carried out using carbon paper as the support for the catalyst ink. CO production occurred with selectivity of ca. 95% and good stability with a maximum partial current density of 165 mA cm^{-2} at -0.92 V vs. RHE (corrected for ohmic drop), in 1 M KOH electrolyte.

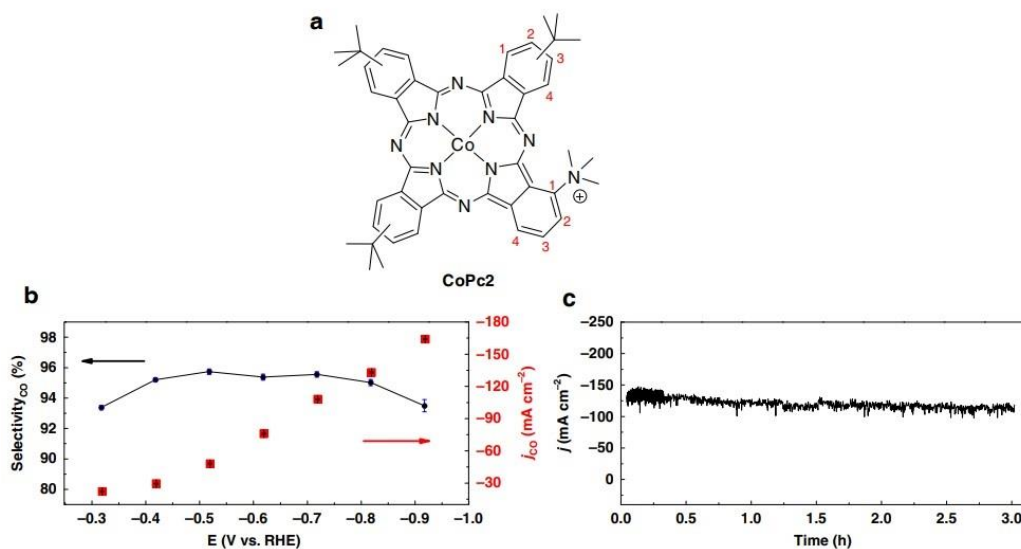


Figure 3. (a) Cobalt phthalocyanine catalyst (CoPc2) bearing one trimethyl ammonium group at position 1 of the isoindole subunits, and three tert-butyl groups (positions 2 or 3) of the other subunits; (b) current density and selectivity for CO production as a function of the potential; (c) bulk electrolysis curve at fixed potential ($E = -0.72$ V vs. RHE). Reproduced with permission from [39].

Among pioneer works, the influence of pressure in CO_2ER using metal-porphyrin catalysts was also investigated [40]. GDEs made of carbon black were impregnated with metal-meso-tetraphenylporphyrin (TPP) catalysts. The catalysts Co- and Fe-TPP, which are relatively active in the electrochemical reduction of CO_2 under atmospheric CO_2 , increased current efficiencies at 20 bar up to 97.4% and 84.6%, respectively. At Cu- and Zn-TPP supported GDEs that showed low activity under atmospheric CO_2 , the current efficiencies for CO_2 reduction increased up to 50.5% and 65.8%, respectively, under 20 bar CO_2 . At these active metal-TPP supported GDEs, the potential of CO_2 reduction shifted positively due to the increase in CO_2 pressure. These results are another example of the influence of high pressure on the enhancement of the electrocatalytic activity of metal-TPPs for CO_2 reduction. Current research trends are investigating electrodes containing porphyrin complexes and other carbon materials. They will be dealt with in Sections 4–6.

3. Mesoporous Carbon-Based Electrodes

One disadvantage of carbon black is its microporous structure. The metal particles may sink inside the micropores, decreasing the electro-catalytically effective surface area. This leads to the development of mesoporous carbons. These materials ($2\text{ nm} < \text{pore sizes} < 50\text{ nm}$) have attracted a lot of attention, due to their regular structure, high surface area, large pore volume and a narrow pore size distribution. They can find potential applications in several fields and their use in CO_2ER was also investigated. While advantages of the use of these materials as catalyst supports in comparison with carbon black has been shown, for instance for the oxygen reduction reaction [41], in CO_2ER several textural properties come into play, and these advantages may not become immediately apparent. Pore structure, existence of heteroatoms in carbon skeleton, hydrophilic or hydrophobic properties need to be first optimized for CO_2ER . One example of these issues is given by Castelo-Quibén et al. [41]. They developed Ni-catalysts by impregnation of mesoporous carbon nanosphere supports and also by Ni doping during the synthesis of the supports. In the case of the catalysts prepared using the later method, catalytic activity was not enhanced by the presence of Ni phases. Ni was incorporated into the carbon matrix in such a way that the metal phase was not accessible to the electrolyte, so the dissolved CO_2 could not reach the metal particle. Catalytic activity was enhanced when the catalysts were prepared by impregnation, as Ni particles were accessible to the electrolyte at the surface of the pores. All the catalysts developed were able to reduce CO_2 to $\text{C}_1\text{--C}_4$ hydrocarbons, even supports, which did not have metal. The highest $\text{C}_1\text{--C}_4$ hydrocarbon production of 117 ppm was obtained for a Ni containing catalyst at $-1.6\text{ V vs. Ag/AgCl}$ with faradaic efficiencies for hydrocarbons of 0.3% in liquid after a 200 min phase electrolysis in batch mode. This work shows that the presence of mesopores has a positive effect in both oxygen reduction reaction and CO_2ER , as it also facilitates ion diffusion at a high speed [42]. Song et al. reported a nitrogen-doped ordered cylindrical mesoporous carbon as a metal-free catalyst for CO_2ER into ethanol. Materials with different configurations were prepared (cylindrical pore structure c-NC and with inverse pore structure i-NC) [43]. The c-NC configuration showed superior selectivity for ethanol. The catalyst ink was brushed onto a porous layer previously painted onto carbon paper. Electrolyses in gas-phase were carried out using 0.1 M KHCO_3 as electrolyte yielded faradaic efficiency of 77% for ethanol at -0.56 V vs. RHE with current densities of ca. 0.25 mA cm^{-2} . These results were attributed to the synergetic effect of the nitrogen heteroatoms and the cylindrical channel configurations, which facilitates the dimerization of key CO^* intermediates and subsequent proton-electron transfers. Figure 4 presents a schematic illustration of c-NC and i-NC for CO_2 electroreduction.

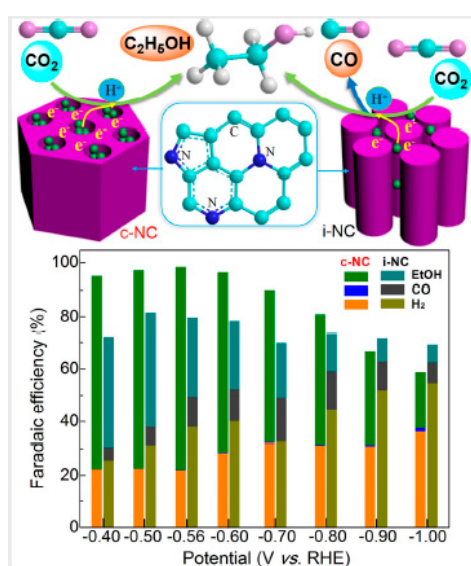


Figure 4. Schematic representation of c-NC and i-NC for CO_2 electroreduction. Reproduced with permission from [43]. Copyright Wiley-VCH, 2017.

Mesoporous N-doped carbon derived by sacrificing metalorganic frameworks (MOF), are also receiving attention. Kuang et al. prepared an N-doped mesoporous carbon from the pyrolysis of Zn-based zeolitic imidazolate framework-8 (ZIF-8) [44]. Electrolysis in liquid phase with 0.1 M KHCO_3 as electrolyte yielded a faradaic efficiency of $\sim 92\%$ for CO and a partial current density for CO of $-6.8 \text{ mA}\cdot\text{cm}^{-2}$, achieved at a potential of -0.58 V vs. RHE. It was concluded that the hierarchical porosity, with large specific surface area and pore volume, can improve the three-phase contact and transport of reactants and products, which can be beneficial for the electro-catalytic CO_2 reduction in the aqueous phase. The synthesis of this type of carbon material, involving the assembly of relative elaborated architectures by using commercial reagents and subsequently sacrificing them through annealing, is expensive and time consuming. It will hardly be cost effective for a commercial application.

4. Carbon Fibers

Macroscopic carbon fibers attached to each other in a form of a matt—carbon cloth (CC)—have low electrical resistance, relatively low cost, and large surface area. This material is widely used for the preparation of electrodes for low temperature fuel cells and was investigated as catalyst support for CO_2 ER.

Morlanés et al. prepared electrodes consisting of perfluorinated cobalt phthalocyanine (CoFPc) immobilized on CC [45]. As this complex also catalyzes O_2 evolution, a two-electrode system was assembled with the same electrodes as cathode and anode, and 0.5 M NaHCO_3 electrolyte in both cathodic and anodic compartment, for liquid phase electrolysis. Current densities in the range of $1\text{--}6 \text{ mA cm}^{-2}$, with faradaic efficiencies of CO $\sim 90\%$ at an applied cell voltage range of ca. $2\text{--}3 \text{ V}$ were achieved. Production rates in the range of $24\text{--}95 \mu\text{mol cm}^{-2} \text{ h}^{-1}$ were observed.

The organometallic complex (fac-Mn(apbpy)(CO)3Br) (apbpy = 4-(4-aminophenyl)-2,20-bipyridine) grafted electrochemically onto CC, was examined as catalyst for CO_2 ER [46]. The catalyst was covalently bonded to CC. A faradaic efficiency of around 60% for CO and 40% for H_2 at -1.35 V vs. Ag/AgCl is achieved together with a partial current for CO of ca. 0.9 mAcm^{-2} in electrolysis carried out in liquid phase with 0.1 M KHCO_3 electrolyte. However, it was shown that even if these materials are made of long fibers, carbon cloths do not possess good electrode properties, due to the existence of double porosity and electrical conduction problems. Thus, the use of such a material as an electrode is not recommended [47].

Carbon nanofibers were also investigated as constituents of cathodes for CO_2 ER. The materials are made of graphene layers, have good electrical conductivity, high surface areas and represent a good compromise between structural and textural properties (low content in micropores and impurities). These nanofibers can be obtained by the decomposition of carbon-containing gases, like methane or carbon monoxide, over small metallic particles as catalysts, typically metals of the iron subgroup. Alternatively, they can be easily synthesized from spinnable polymer precursors, such as polyacrylonitrile [48]. Through this process, fibers of higher purity and without traces of metals that can influence catalysis can be obtained.

Magdesieva et al. investigated several porphyrin and phthalocyanine transition metal complexes supported on activated carbon fibers (surface area $1400\text{--}1500 \text{ m}^2 \text{ g}^{-1}$) and on activated carbon (surface area $2000 \text{ m}^2 \text{ g}^{-1}$) [49]. GDEs were prepared by pressing a paste containing the supported metal complexes with the gas diffusion layer. The partial current densities for CO production, measured in 0.5 M KHCO_3 solutions, were up to 70 mA cm^{-2} at -1.5 V vs. SCE. The catalysts supported on activated carbon fibers showed better performance in CO_2 ER than those supported on activated carbon for smaller complex sizes that could be adsorbed on the surface of the nanopores of the activated carbon fibers. On the contrary, for larger complexes the catalysts supported on activated carbon showed better performance, due to the wider pores (microporosity) available in this material.

Kumar et al., using N-doped carbon nanofibers (CNFs) directly as electrode, reduced CO_2 into CO in liquid phase at -0.573 V vs. RHE with 98% faradaic efficiency and current densities near 0.5 mAcm^{-2} [50]. An aqueous solution of the ionic liquid 1-butyl-3-methyl-imidazolium tetrafluoroborate was used as electrolyte. The activity of a nitrogen-free catalyst (graphite) under

similar experimental conditions showed negligible activity for CO₂ER. This electrolyte was chosen due to the high CO₂ absorption capacity of some ionic liquids [51]. The N-doped CNFs were synthesized by pyrolysis of electrospun nanofiber mats of heteroatomic polyacrylonitrile (PAN) polymer.

Yang et al. prepared N-doped carbon fibers with a core of Ag nanowires of 70–80 nm diameter [52]. The objective was to increase the local concentration of CO₂ around the Ag nanowires (AgNWs), due to its porous structure. AgNWs were well dispersed in Tris buffer (pH = 8.5), which was followed by adding a specific amount of dopamine (DA) to form the polydopamine (PDA) shell under continuous stirring. Subsequently, the material was carbonized under argon atmosphere at different temperatures. The PDA decomposed, creating the N-doped carbon layer. Figure 5 shows schematically the preparation process of these catalysts. A synergistic effect was observed between the Ag nanowires and the N-doped carbon shell. The working electrodes were prepared by drop-casting the catalyst ink containing the wrapped Ag nanowires on carbon paper. Electrolysis in liquid phase with 0.1 M KHCO₃ electrolyte showed that CO and H₂ were the major products formed and no liquid products were detected. The higher faradaic efficiency of 96% was obtained at –0.8 V vs. RHE with CO formation rates of 774 μmol m^{–2} s^{–1}. The CO formed was further reacted with organic compounds to form organic carbonyls.

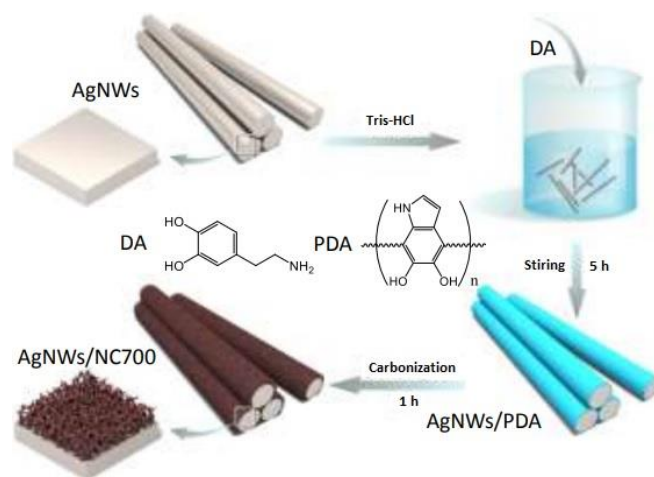


Figure 5. Schematic representation of the synthesis of N-doped carbon fibers with a core of Ag nanowires employing a carbonization temperature of 700 °C (AgNWs/NC700). Reproduced with permission from [52]. Copyright Wiley-VCH, 2018.

5. Graphene

Graphene (GN) can be prepared using chemical-, electrochemical- or mechanical-exfoliation of graphite. This constitutes the so-called bottom down approach. In the bottom up approach chemical synthesis or chemical vapor deposition is employed. This nanomaterial has a two-dimensional honeycomb lattice of sp² hybridized carbon atom. It can be grown in different morphologies including monolayer and multilayer graphene nanosheets, zero-dimensional graphene quantum dots, graphene nanoflowers and graphene nanoribbons. Since its first laboratory synthesis in 2004, it has been a hot topic of research, due to its remarkable huge surface area, high electrical conductivity, high thermal conductivity, good chemical and mechanical properties [53]. Among other end uses, these characteristics make graphene very interesting for catalytic applications, and thus, it has also been investigated as electrode component in electro-reduction of CO₂. As in the case of carbon black, graphene and its modifications were utilized having different strategies in mind. Interestingly, synergies between metal catalysts and these carbon materials were disclosed. An example of metal-support synergy was reported by Rogers et al. [54]. These authors revealed that the structural and electronic properties of the graphene nanoribbon (GNR) matrix increased the electrochemically active surface area of Au nanoparticles assembled on this matrix. This material showed better activity for CO production

(36.8 A g⁻¹), stability and lower overpotentials than Au nanoparticles supported on carbon black (6.4 A g⁻¹). Faradaic efficiencies for CO were >70%.

Geiously et al. also found a synergy between Cu₂O and graphene, when GN was used as the support of the nanoparticles [55]. An electrode consisting of an ink containing the composite of GN/Cu₂O with an average particle size of 20–50 nm, coated on copper foil, was more active than the electrode without graphene. A current density of approximately 12.2 mAcm⁻² at –1.7 V vs. Ag/AgCl was obtained using linear sweep voltammetry, which was higher than for a Cu₂O electrode (8.4 mAcm⁻²). Electrolysis in liquid phase with 0.5 M KHCO₃, as electrolyte yielded ethanol (~0.34 ppm) as predominant product at –0.9 V vs. Ag/AgCl with a faradaic efficiency up to 9.93%. No ethanol was detected when the electrode containing only Cu₂O was used.

Pristine graphene is not active for CO₂ER, but, by introducing atomic defects through heteroatom doping, it can be made active for this reaction [56]. Wang et al. described an electrode with a catalyst ink including N-doped graphene (NG) brushed on to carbon paper, as metal free catalyst [57]. These authors reported a steady current density at around –7.5 mA cm⁻² throughout the 12 h electrolysis in liquid phase carried out at an applied potential of –0.84 V vs. RHE with faradaic efficiencies for formate varying in the range of 70–63% in 0.5 KHCO₃.

Wu et al. used N-doped 3D-graphene (NG) foam as a metal-free catalyst to reduce CO₂ to CO in gas phase [58]. The ink containing N-doped graphene foam was sprayed onto the gas diffusion layer. A current of ca. 1.8 mAcm⁻² (FE for CO ca. 70% and FE for HCOOH of 3.0%) was obtained at an applied potential –0.58 V vs. RHE in 0.1 M KHCO₃. DFT calculations confirmed the pyridinic N as the most active site for CO₂ reduction in accordance with experimental results.

Boron doping is much less investigated than nitrogen doping. Sreekanth et al. prepared electrodes of B-doped graphene ink drop-casted on glassy carbon and reported a faradaic efficiency of CO₂ reduction to formate of 66% in liquid phase, at –1.4 V vs. SCE with a current density of ca. 0.5 mAcm⁻² [56].

N-doped graphene has also attracted a lot of attention as an electrode support displaying metal-support synergies that increase catalytic activity, as described below. Li et al. reported that N-doped graphene could reduce CO₂ to formate with a mass activity of 7.7 A g⁻¹ and maximum faradaic efficiency of 65% at –0.9 V vs. RHE in electrolysis carried out in 0.5 KHCO₃ electrolyte, with hydrogen as the other electrolysis product [59]. Furthermore, it was reported that electrolysis carried out with 7 nm Cu nanoparticles dispersed on N-doped graphene yielded hydrogen, formate, methane, ethylene and ethane, but no CO. Ethylene was predominantly formed and formate production suppressed at –0.9 V vs. RHE with a faradaic efficiency of 19% and a mass activity for ethylene of 2.9 A g⁻¹Cu. The mass activity for ethylene of Cu nanoparticles dispersed on Ketjen carbon black prepared for comparison was ca. 0.5 A g⁻¹Cu.

Recently Han et al. prepared graphene with a large number of topological defects using a nitrogen removal method [60]. This material presented numerous catalytically active sites, high electronic conductivity and strong adsorption of CO₂. A cathode was prepared by loading an ink containing the defected graphene on carbon paper. Electrolysis carried out in liquid phase using 0.1 M KHCO₃ as electrolyte was undertaken. Faradaic efficiency of ~84% and a partial current density for CO of 1.3 mA cm⁻² at –0.6 V vs. RHE were reported. This current was higher than the one obtained with pristine graphene, nitrogen-doped graphene and edge-rich graphene electrodes.

Importantly, Chai et al. predicted using both density functional theory (DFT) and ab initio molecular dynamic calculations that the interplay of N-doping and curvature can effectively tune the activity and selectivity of graphene/carbon-nanotube (CNT) catalysts [61]. The graphene catalyst without curvature showed strong selectivity for CO/HCOOH production, whereas the CNT with a high degree of curvature was effective for both CH₃OH and HCHO production. Curvature was also very influential to tune the overpotential for CO formation.

6. Graphene Derivatives

Graphene oxide (GO) is one important graphene derivative. It contains several functional groups, such as epoxy, hydroxyl, carbonyl and carboxyl groups. GO has weak electrical conductivity, due to the presence of hydrophilic functional groups. One way to increase its electrical conductivity is by removing oxygen containing functional groups to produce reduced graphene (rGO).

One approach to achieve high mass activities of catalysts is to decrease particle size. This approach was also investigated for graphene derivatives-based electrodes. It was observed that decreasing particle size below a certain limit favors H₂ evolution, due to abundant low coordinated sites of the very small nanoparticles [62,63]. This results in poor selectivity towards CO₂ reduction products. Zhao et al. circumvented this problem by supporting ultra small (ca. 2.4 nm) Au NPs on rGO sheets [64]. They obtained Au-specific mass activities (>100 A g⁻¹) and good faradaic efficiencies (32–60%) for the CO₂ to CO conversion at moderate overpotentials (450–600 mV). Furthermore, the Au NPs were modified with amines with the capability of CO₂ adsorption and suppressing H₂ evolution. This modification allowed faradaic efficiencies to be increased to 59–75%. An amine structure dependent effect in selectivity was revealed. Among all the modifiers, oleylamine exhibited the highest CO selectivity with CO partial current densities of ca. 6 mAcm⁻² at –0.7 V vs. RHE. The catalyst was prepared by dropping the catalyst ink containing the rGO composite on a layer of Vulcan carbon black painted on a surface of carbon paper. CO₂ reduction was carried out in liquid phase, in 0.1 M KHCO₃.

Cu nanowires of 20 nm width were selective for CH₄ (FE of 55%, partial current densities near 8 mA cm⁻²) at –1.25 V versus RHE in 0.1 M KHCO₃; however, selectivity was sensitive to morphological changes. Wrapping the nanowires with rGO stabilized the catalyst preserving morphology and selectivity [65]. Electrodes were prepared by loading the wrapped Cu nanowires in rGO in Ketjen carbon black, and then, the ink solution was spread onto carbon plates.

A further study of metal particles supported on rGO was presented by Hossein et al. [66]. These authors prepared a catalyst in which adenine was bonded on the surface of rGO via diazonium reaction. Adenine-rGO was drop-casted on a glassy carbon substrate. Then, Pt was deposited on the surface of adenine-rGO to prepare the Pt@Adenine-rGO working electrode. In acidic media, nitrogen-containing heterocyclic on the structure of adenine was protonated and allowed the formation of hydrogen atoms on the surface of Pt, which, interacting with carbon dioxide, reduced CO₂ to methanol. This alcohol was obtained as the main product with a faradaic efficiency up to 85% and a current density of 0.5 mA cm⁻². The electrolyte used was 0.1 M KNO₃.

Ning et al. prepared a composite of cuprous oxide (Cu₂O) nanocubes on nitrogen-doped reduced graphene oxide (NrGO) to fabricate a Cu₂O/NrGO composite [67]. An ink of this composite was prepared, smeared and let dry on a glassy substrate to produce the working electrode. Electrolysis in 0.1 M KHCO₃ exhibited a faradaic efficiency of ethylene (19.7%) at –1.4 V vs. RHE with stable current density of 12 mAcm⁻². The mass activity of Cu₂O supported on reduced graphene oxide towards C₂H₄ formation reaches as high as 136.1 mmol h⁻¹ g⁻¹, which was more than 24-fold of pristine Cu₂O. The pyridinic N in reduced graphene oxide was supposed to behave synergistically with Cu₂O, leading to an enhancement of activity and durability of Cu₂O for electrocatalytic CO₂ reduction to ethylene. Figure 6 shows SEM images of reduced graphene oxide (rGO) the Cu₂O/NrGO composite catalyst and its constituents.

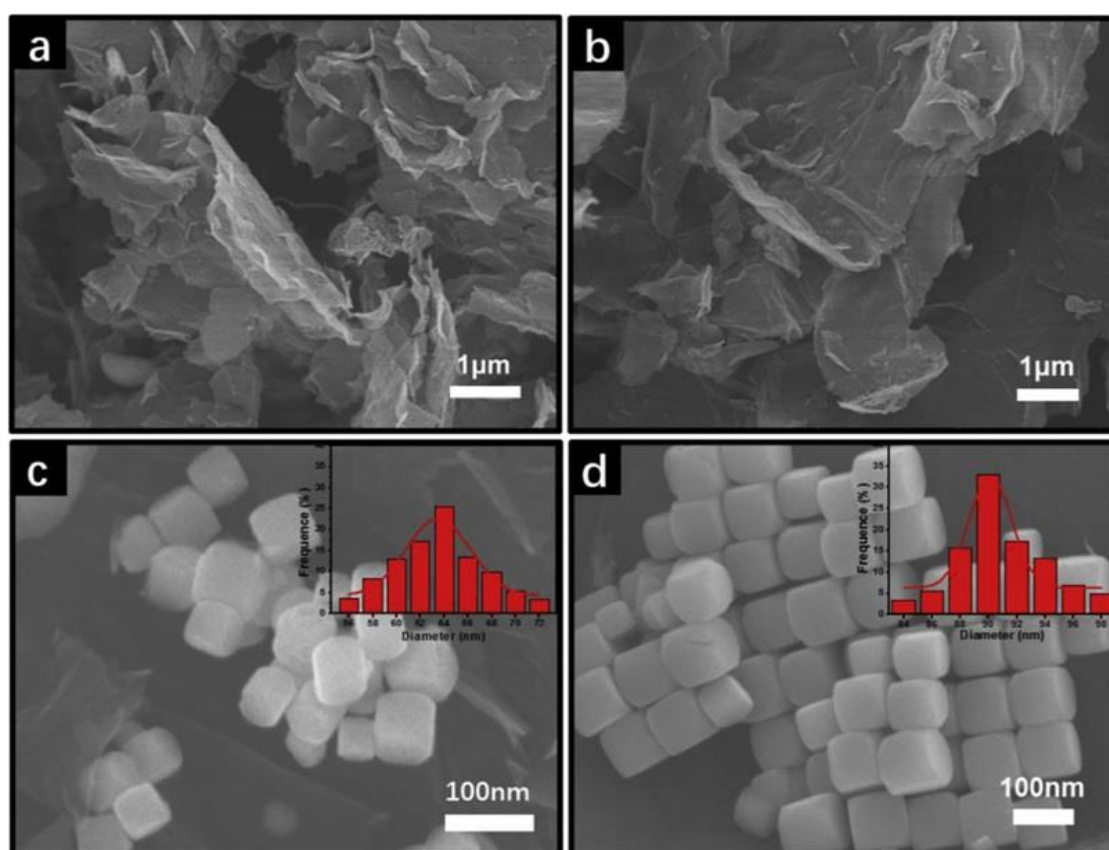


Figure 6. SEM images of (a) reduced graphene oxide (rGO); (b) N-doped reduced graphene oxide (NrGO); (c) $\text{Cu}_2\text{O}/\text{rGO}$ composite catalyst; (d) $\text{Cu}_2\text{O}/\text{NrGO}$ composite catalyst. Reproduced with permission from [67]. Copyright Elsevier B. V., 2019.

Attaching molecular catalysts to graphene derivatives was also investigated. Zhou et al. prepared a re-functionalized porphyrin on graphene oxide that was then deposited onto a glassy carbon electrode (GC) for CO_2 ER into syngas [68]. The complexes *fac*- $\text{M}(4\text{-amino-bipy})(\text{CO})_3\text{X}$ ($\text{M} = \text{Mn}$ and $\text{X} = \text{Br}$ or $\text{M} = \text{Re}$ and $\text{X} = \text{Cl}$, $\text{bipy} = 2,2'\text{-bipyridine}$) were synthesized and immobilized on GrO via diazonium grafting. The prepared electrode catalyzed CO_2 to CO conversion with an optimized turnover frequency of up to 4.44 s^{-1} for CO generation. The electrolyte used was aqueous acetonitrile. Mass transfer limitations affected activity. Stirring the electrolyte solution produced a threefold increase of the reaction rate. Co-generation of H_2 using the bare glassy carbon electrode enabled the production of syngas with tunable CO/H_2 ratios, by changing the CO_2 diffusion rate, or by deliberately adjusting the surface coverage of the catalyst at the electrode.

Choi et al. prepared a porphyrin/graphene framework (FePGF) composed of Fe(III) tetraphenyltrimethylammonium porphyrin and reduced liquid crystalline graphene oxide [69]. A high surface area carbon fiber paper was used as a substrate for FePGF catalyst. A current density was reported of 1.68 mA cm^{-2} with 98.7% CO faradaic efficiency at an overpotential of 430 mV for 10 h with a cathodic energy efficiency of 60.9%, corresponding to a turnover frequency of 2.9 s^{-1} and 104 400 turnover number. These authors also examined the effect of the degree of GO reduction. The catalyst FePGF appeared to offer the required balance between electrostatic interaction and reduced character, yielding both high catalytic efficiency and long-term stability.

Yuan et al. investigated functionalized GO as metal-free catalyst. Pyridine derivatives, such as 4-hydroxypyridine, 4-aminopyridine, 8-hydroxyquinoline, 5-amino-1,10-phenanthroline and pyridoxine (vitamin B6), were grafted on GO sheets [70]. An ink containing the catalyst was prepared and spread over carbon paper for cathode assembly. The GO-VB6 catalysts demonstrated

superior activity for the electrochemical reduction of CO₂ to ethanol than the modifications with the other four pyridine derivatives on GO sheets. The catalytic active of GO-VB6 was affected by the pyridinic N contents in the GO-VB6 catalysts. The experimental data revealed that pyridinic N is the active site for CO₂ER. Besides, the catalytic activities of pyridine derivative modified GO exhibit distinct performances, which are not only closely related to the pyridinic N contents of the GO-X, but also the structure of grafted pyridine derivatives. Electrolysis in liquid phase was carried out in 0.1 M KHCO₃ electrolyte. The best results were observed for GO-VB6 with an N content of around 2.32% on the surface of GO sheets, which produce the maximum FE of ethanol of approximately 37%, with a partial current density of ca. 0.25 mA cm⁻² at -0.4 V vs. RHE.

Three dimensional electrodes have been proposed to overcome the low CO₂, electrolyte accessibility to catalytic sites and mass transfer limitations. rGO hydrogels have been suggested, among others, for electrochemical applications, due to their good electrical conductivity, suitable mechanical properties and thermal stability [71]. The highly porous structures of hydrogels containing large amounts of water favor electrolyte accessibility and wettability in aqueous media. Choi et al. have developed an iron porphyrin-based rGO hydrogel, prepared via a hydrothermal method, as a three-dimensional catalyst for CO₂ER [72]. This catalyst was deposited into a reticulated vitreous carbon electrode. At -0.39 V vs. RHE, CO₂ was reduced to CO with ca. 96% faradaic efficiency and a stable current density of 0.42 mAcm⁻² in a 20 h electrolysis, carried out in 0.1 M KHCO₃.

7. Carbon Nanotubes

Carbon nanotubes are long, thin graphitic cylinders, which, if simplified, can be regarded as a sheet of graphite rolled into a cylinder. They can have a single cylindrical wall (SWNTs) or multiple walls (MWCNTs), with cylinders inside the other cylinders. Electrodes composed of carbon nanotubes have generated much interest because of their high conductivity, large surface area and their ability to facilitate catalytic processes. These materials have also been investigated for CO₂ER following different strategies.

Supporting metal nanoparticles on CNT was one of the strategies followed to increase catalyst performance. Feng et al. showed that surface-area-normalized activity for CO₂ reduction is linearly correlated with grain boundary (GB) surface density on Au/CNT (Figure 7) [73]. They proposed grain boundary engineering as a strategy to improve the catalytic activity of metal nanoparticles. This correlation led to an understanding of the different current densities and faradaic efficiencies reported for Au nanoparticles of different size and shape [19–21]. Au/CNT electrodes were prepared by depositing Au nanoparticles on a CNT film using electron beam evaporation. The Au/CNT films were rolled into yarns and connected to Au wires. Electrolyses in liquid phase were carried out in 0.5 M, and NaHCO₃, CO and H₂ were the major products formed with current densities in the order of magnitude of μAcm⁻².

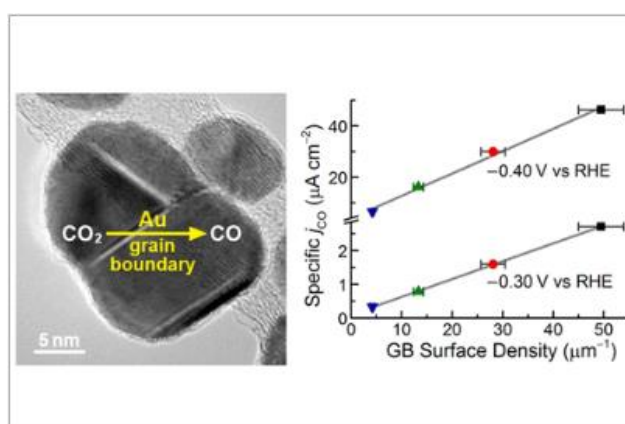


Figure 7. Correlation between current density and grain boundary (GB) surface density. Reproduced with permission from [73]. Copyright American Chemical Society, 2015.

Recently, a catalyst was prepared consisting of Au nanoparticles supported on poly(2,2'-(2,6-pyridine)-5,5'-bibenzimidazole) polymer (PyPBI) wrapped multiwall carbon nanotubes as the cathode catalyst [74]. The catalyst ink containing the prepared catalyst multiwall carbon nanotubes/PyPBI/Au was airbrushed on the gas diffusion layer. Figure 8 shows a schematic representation of the catalyst and of the microfluidic electrolysis cell used. This catalyst was further improved, and high j_{CO} (~ 99 , 158 mA cm^{-2}) was obtained at low overpotential (~ 0.70 , 0.94 V) and high CO energetic efficiency (~ 63.8 , 49.4%), respectively [75]. The performance was stable for at least 8 h. The observed high activity was due to a high electrochemically active surface area, in combination with the low loading of the highly-dispersed Au nanoparticles.

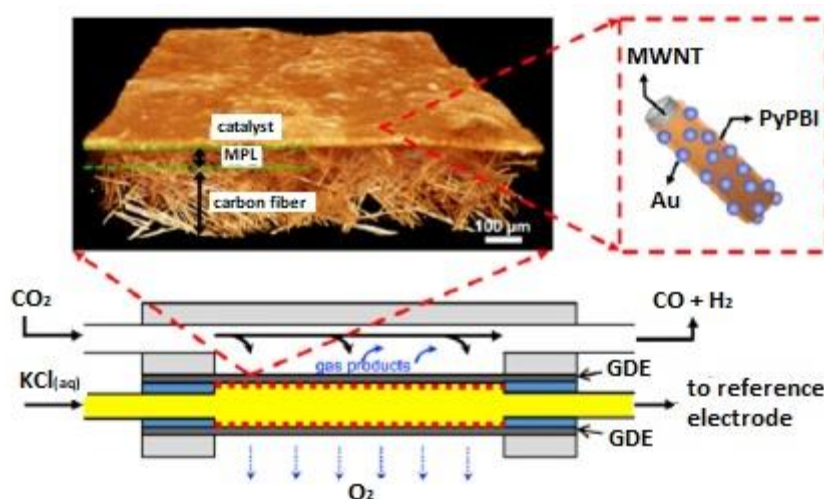


Figure 8. Schematic representation of the Au catalyst supported on polymer-wrapped multiwall nanotubes (MWNT/PyPBI/Au). Top left: reconstructed 3D view obtained from MicroCT data. Bottom: schematic representation of the microfluidic electrolysis cell used. Reproduced with permission from [74]. Copyright Wiley-VCH, 2017.

Zhao et al. compared differently prepared catalysts of tin oxide particles supported on multiwall carbon nanotubes [76]. The cathode was prepared by pressing the catalytic ink, also containing carbon black, onto a stainless steel mesh. Liquid phase electrolysis carried out in 0.1 M KHCO_3 yielded maximum faradaic efficiencies of 60% with 25% energy efficiency for HCOOH formation and current densities in the range of $5\text{--}10 \text{ mA cm}^{-2}$. Different morphologies of the particle agglomerates made little difference in the electrocatalytic selectivity and activity.

Results that stand out among the studies of metal nanoparticles supported on carbon nanotube catalysts are presented in the work of Ma et al. [77]. The authors investigated MWCNTs containing Ag nanoparticles in an optimized flow system. The electrode was prepared by air brushing the ink containing MWCNT and Ag nanoparticles onto the gas diffusion layer. Electrolysis in gas-phase yielded faradaic efficiencies of CO of 95%, a current density of 350 mA cm^{-2} and energy efficiency of 45%. An electrochemical impedance spectroscopy study revealed that this mixed catalyst had lower resistance to charge transfer/higher charge transfer rate, which enhanced the electrochemical reaction.

Bashir et al. studied the effect of metal loading of tin oxide supported on acid functionalized multiwall carbon nanotubes ($\text{SnO}_2/\text{MWCNT}$) [78]. The cathode was prepared by adding the catalyst ink layer by layer onto carbon paper. Liquid phase electrolysis was carried out in 0.5 M NaHCO_3 . The best result was obtained for an electrode with 20% weight of SnO_2 . Formate faradaic efficiency of 27.2% was achieved with a current density of 80 mA cm^{-2} at a potential of -1.7 V vs. SCE .

Marepally et al. prepared catalysts consisting of Cu nanoparticles deposited onto commercial carbon nanotubes, preliminarily activated with HNO_3 to create oxygen functional groups on their external surface (o-CNTs) [79]. These catalysts were shown to be active in C–C coupling. The catalyst was deposited on a gas diffusion layer and electrolysis was carried out in gas phase using 0.5 M KHCO_3

as electrolyte, applying a constant bias of -2V . Results showed that Cu NPs supported over CNTs greatly depend on the method of preparation. The catalysts prepared using the method developed by these authors (CuCNT) gave better performances than the electrodes prepared via conventional impregnation methods (CuCNT-Imp). The higher production of methanol for CuCNT with respect to CuCNT-Imp (0.98 vs. $0.31 \mu\text{mol h}^{-1}$) was ascribed in part to the higher surface area of Cu NP, as the prepared CuCNT showed smaller particles, but also to the state of oxidation of Cu (Cu^0 in CuCNT). The reduction of Cu^{II} to Cu^0 in CuCNT-Imp during electrolysis likely involves only the shell of the particles, with formation of a core-shell structure (Cu^0 in the external surface and Cu^{II} in the core of the particle) that influences the electronic properties of the surface and consequently the reactivity. Moreover, C_2 - C_3 products, ethanol, acetic acid, isopropanol, and acetone, were obtained with the developed catalysts, showing the possibility of C-C bond formation.

Molecular catalysts were also investigated in combination with carbon nanotubes. Walsh et al. prepared an electrode consisting of a complex *fac*-Mn(apbpy)(CO)3Br, apbpy = 4-(4-aminophenyl)-2,2'-bipyridine cast on a Nafion membrane on a glassy carbon substrate [80]. When MWCNT was also cast on the membrane (MWCNT/Nafion/[Mn(bpy)(CO)3Br]), a 10-fold enhancement in current density in cyclic voltammetry measurements was observed under CO_2 at -1.4 V vs. Ag/AgCl at pH 7 (3 mA cm^2 vs. 0.3 mA cm^2) using phosphate buffer pH 7 as electrolyte. This enhancement was caused by the increase in the electroactive concentration of the complex, due to the large area of the MWCNT support. Further progress was reported with the complex [Mn(bpy(tBu)₂)(CO)3Br] (2, where (bpy(tBu)₂) = 4,40-di-tert-butyl-2,20-bipyridine). At neutral pH, a current density of 2.65 mA cm^{-2} at -1.5 V vs. SCE, a selectivity towards CO_2 ($\text{CO}:\text{H}_2 = 0.33$) and a faradaic efficiency for CO of 24% were achieved [81].

Aoi et al. investigated CO_2 ER using a glassy carbon electrode modified with a cobalt(II) chlorin complex, adsorbed on multiwall carbon nanotubes, in liquid phase electrolysis at an applied potential of -1.1 V vs. NHE to yield CO with a faradaic efficiency of 89%, with hydrogen production accounting for the remaining 11% in aqueous Na_2SO_4 at pH 4.6 [82]. After 30 h of electrolysis, 0.4 mmol cm^{-2} of CO were produced. When MWCNTs were replaced by rGO, which is planar, as a support material of CoII(Ch), the CO and H_2 yields became much smaller. They concluded that the three-dimensional assembly of MWCNTs with CoII(Ch) on the electrode surface may play an important role for the selective electrocatalytic reduction of CO_2 to CO.

Cobalt meso-tetraphenylporphyrin (CoTPP) was directly immobilized onto CNT via adsorption [83]. The working electrode was prepared by drop-casting the suspension containing CoTPP and CNT on the glassy carbon electrode. Four hours of electrolysis in liquid phase with 0.5 M KHCO_3 as electrolyte at -1.35 V vs. SCE accumulated $189\text{ }\mu\text{mol cm}^{-2}$ of CO.

Zhang et al. introduced cyano groups in the cobalt phthalocyanine molecule (CoPc-CN). These molecules were uniformly anchored on carbon nanotubes [84]. The working electrodes were prepared by drop-drying the catalyst inks onto carbon fiber paper. Electrolysis in liquid phase using as electrolyte 0.1 M KHCO_3 near neutrality yielded a current density of 15.0 mA cm^{-2} and faradaic efficiency for CO >95% at -0.63 V vs. RHE (overpotential of 0.52 V , IR corrected).

In order to increase the structural stability of molecular catalysts immobilized on CNTs, Han et al. prepared a hybrid catalyst material consisting of a CNT core and cobalt polyphthalocyanine (CoPPc) sheath [85]. The catalyst powder was blended with Ketjen black carbon and Nafion polymer binder and drop-cast onto carbon fiber paper (CFP) as the working electrode. Extensive cross-linking of CoPPc on the conductive support not only suppresses the aggregation of organic molecules and enlarges their electrochemically active surface area but also contributes to their physical and chemical robustness. Electrolysis in liquid phase conducted in 0.5 M KHCO_3 electrolyte yielded at least 24 h stable current density of 18.7 mA cm^{-2} and faradaic efficiencies for CO >80% at -0.5 V vs. RHE (0.43 V overpotential).

Wang et al. prepared a catalyst ink containing the Co complex of the planar tetradentate ligand 2,2':6',2'':6'',2'''-quaterpyridine [$\text{Co}(\text{qpy})^{2+}$] and the MWCNT [86]. The ink was drop-casted on carbon paper. Electrolysis in liquid phase using this cathode in 0.5 M NaHCO_3 (pH 7.3) yielded CO with 100%

faradaic efficiency with a current density of 9.3 mA cm^{-2} that could be sustained for several hours at -0.48 V vs. RHE (340 mV overpotential).

Wang et al. prepared porous carbon membranes that were used directly as electrodes. These membranes consisted of multiwalled carbon nanotubes embedded in an N-doped carbon membrane matrix [87]. In these membranes the macropores provide mass transport highways while the mesopores and micropores provide a large surface area and high population of spatially accessible electroactive sites for CO_2ER . The nitrogen species incorporated into the carbon framework constitute the active sites for the reaction. The faradaic efficiency for the production of formate was 81% at -0.8 V vs. RHE , the remaining products were CO and H_2 . Electrochemical stability of at least 36 h and current densities of ca. 6 mA cm^{-2} were obtained in potential controlled electrolysis in 0.1 M KHCO_3 .

8. Nitrogen-Doped Carbon Nanotubes

Heteroatom doping, in particular N-doping of carbon nanotubes (N-CNT), was also an approach used for developing N-CNT-based catalysts. Zhang et al. drop-casted multiwall CNT on a glassy carbon electrode [88]. The CNT was doped with nitrogen and oxygen. Oxygen doped CNT and CNT electrodes mainly gave H_2 as the product ($>90\%$) with a small amount of CO ($<1\%$). A polyethyleneimine (PEI) overlayer that is used as CO_2 absorbent was applied to N-CNT/GC by attachment to the surface of CNT based on van der Waals forces. PEI-N-CNT exhibited the most positive onset potential for CO_2 reduction. Electrolysis in 0.1 M KHCO_3 at -1.8 V vs. SCE for 24 h exhibited a steady-state catalytic current density of 7.2 mA cm^{-2} . Formate was the dominant product formed with a faradaic efficiency of 85%.

Wu et al. showed that N-doped CNTs were active for CO_2ER into CO at a significantly lower overpotential than pristine CNTs. GDEs electrodes were prepared by spraying an ink containing N-doped multiwall carbon nanotubes with a bamboo shape on a gas diffusion layer [89]. The bamboo-like structure is a characteristic feature of nitrogen atom defects in CNTs, which originates from the formation of a positive curvature surface during substitution of nitrogen atoms into the graphitic structure [90]. The long-term performance of N-doped CNT catalysts at constant applied potential of -0.8 V vs. RHE for 10 h was tested. A stable current density at around -1.0 mA cm^{-2} was obtained. FE of CO fluctuated slightly around 80%.

Sharma et al. synthesized N-doped CNTs with various surface structures and nitrogen contents by choosing different precursors and controlling the growth temperature [91]. Electrodes were prepared by spraying the catalyst ink over a carbon gas diffusion layer. The catalytic activity of these N-doped CNTs was found to depend upon the nature of nitrogen defects and defect density. The presence of graphitic and pyridinic N defects significantly decreased the absolute overpotential and increased the selectivity towards CO formation in comparison to pristine CNTs. The most active N-doped CNT exhibited a faradaic efficiency of 80%, CO partial current densities of ca. -2 mA cm^{-2} at a cell voltage of -1.05 V (corrected for IR drop) owing to the highest pyridinic (ca. 1.1 at%) and graphitic N (ca. 3.5 at%) content (see Figure 9). Furthermore, pyrrolic N defects seem to have little or no impact on CO_2ER activity, in accordance with DFT calculations [92].

Cui et al. have conceived a steam etching strategy to tune the nitrogen dopant types and levels to promote CO_2ER [93]. They prepared nitrogen-doped carbon-wrapped carbon nanotubes (CN-H-CNT) and transformed their nitrogen type via steam etching (percentages of pyridinic, graphitic, and oxidized N atoms decrease to 9.8%, 24.9% and 9.4%, respectively, while pyrrolic N increases substantially from 22.1% to 55.9%). CN-H-CNT films on silicon wafer substrate were employed directly as electrodes. Electrolysis in liquid phase using 0.1 M KHCO_3 as electrolyte was undertaken. Maximum faradaic efficiency of ca. 88% toward the formation of CO at -0.5 V vs. RHE was reported. At this potential, current density (in absolute value) slowly decreased from ca. -0.5 mA cm^{-2} at the start of electrolysis, up to a ca. 0.1 mA cm^{-2} during 7 h of electrolysis.

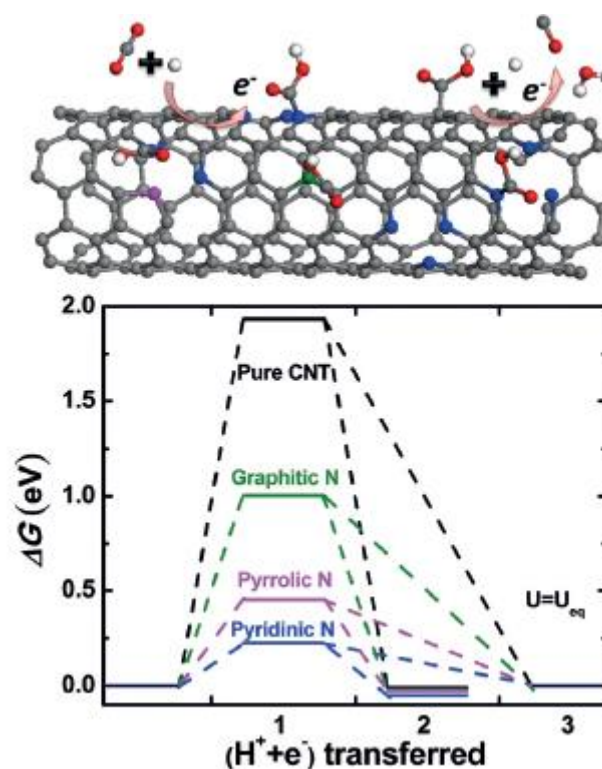


Figure 9. Schematic illustrating CO formation on the N-CNTs and free-energy diagram at equilibrium potential for CO₂ reduction on different N defects, that is, pyridinic, pyrrolic, and graphitic N in comparison to pristine CNTs. C, O, and H atoms are represented by gray, red, and white spheres, while pyridinic, pyrrolic, and graphitic N defects are shown using blue, pink, and green spheres, respectively. Reproduced with permission from [91]. Copyright Wiley-VCH, 2015.

Liu et al. fabricated a 3D electrode by growing N-doped CNTs in situ on a stainless-steel mesh (SS) with only melamine as the nitrogen and carbon sources [94]. Electrolysis in liquid phase was carried out using 0.1 M KHCO₃ as electrolyte. This integrated N-doped CNTs/SS electrode was used directly as working electrode to produce syngas with an FE of 75% for CO with current densities of 2 mAcm⁻² at -1.1 V vs. Ag/AgCl. The H₂/CO ratio could be controlled by the pyrolysis temperature of the N-doped CNT preparation process or by the applied potential. Ratios in the range of 1–3 were obtained.

The performances of electrolytic systems using the carbon materials referred to in this work are listed in Table 1.

Table 1. Performance of electrolytic systems using the carbon materials referred in this work.

Types of Carbon	Catalyst	Current Density (mA/cm ²)	Potential/Voltage	CO ₂ RR Products	Faradaic Efficiency	Reference
Supported Metal and Metal Derived Particles						
Carbon Black	Pb on Vulcan 72	115	−2.7 to −3.0V vs. SCE	Formic acid	97%	Mahmood et al. [6]
	Cu	667	−4.75 V vs. Ag/AgCl	Ethene	53%	Cook et al. [11]
	Cu	300	−1.25 V vs. SHE	Ethylene and ethanol	-	Ikeda et al. [7]
	Ru-Pd alloys	80	−1.1V vs. SHE	Formic acid	90%	Furuya et al. [10]
	Pt	600	−1.93 V vs. Ag/AgCl	Methane	38.8%	Hara et al. [13]
	Au, 8 nm NP	3A/g	−0.67 V vs. RHE	Carbon monoxide	90%	Zhu et al. [19]
	Au 500 nm nanowires	8	−0.35 V vs. RHE	Carbon monoxide	94%	Zhu et al. [20]
	Au25 Clusters	-	−1 V vs. RHE	Carbon monoxide	100%	Kauffman et al. [21]
	Triangular Ag nanoplates	1.25	−0.86 V vs. RHE	Carbon monoxide	97%	Liu et al. [22]
	Cysteamine anchored 5 nmAg nanoparticles	1	−0.35 V vs. RHE	Carbon monoxide	~80%	Kim et al. [23]
	Core/Shell Cu/SnO ₂ Structure	4.6	−0.7 V vs. RHE	Carbon monoxide	93%	Li et al. [24]
	Pd 5 nm nanoparticles	2.2 to 4.15	>−0.2 V vs. RHE	Formic acid	>95%	Min et al. [29]
	Sn nanoparticles	200	−1.4 V vs. Ag/AgCl/4 V cell voltage	Formic acid	54.1%	Del Castillo et al. [30]
	Ni nitride	23.3	−0.90 V vs. RHE	Carbon monoxide	92.5%	Hou et al. [31]
	Ag 20 nm nanoparticles	200	3 V cell voltage	Carbon monoxide	98%	Liu et al. [33]
Molecular Catalysts						
Mesoporous Carbon	Co-Phthalocyanine	80	−4.39 V vs. Ag/AgCl	Carbon monoxide	100%	Savinova et al. [35]
	Co-Phtahlocyanine	137 22	−2.2 V vs. SCE −1.5 V vs. SCE	Carbon monoxide	14% 100%	Mahmood et al. [36]
	Co Phthalocyanine2	165	−0.92 V vs. RHE	Carbon monoxide	95%	Wang et al. [39]
	Carbon nanospheres impregnated with Ni particles	-	−1.6 V vs. Ag/AgCl	C ₁ -C ₄ hydrocarbons	0.3%	Castelo-Quibén et al. [41]
	Nitrogen doped mesoporous carbon	0.25	−0.56 V vs. RHE	Ethanol	77%	Song et al. [43]
	mesoporous N-doped carbon	6.8	−0.58 V vs. RHE	Carbon monoxide	~92%	Kuang et al. [44]

Table 1. Cont.

Types of Carbon	Catalyst	Current Density (mA/cm ²)	Potential/Voltage	CO ₂ RR Products	Faradaic Efficiency	Reference
Supported Metal and Metal Derived Particles						
Carbon Fibers	CoFPC immobilized on carbon cloth	1–6	2–3 V cell voltage	Carbon monoxide	~90%	Morlanés et al. [45]
	fac-Mn(apbpy)(CO) ₃ Br attached on carbon cloth	0.9	–1.35 V vs. Ag/AgCl	syngas	60% for CO	Rotundo et al. [46]
	porphyrin and phthalocyanine	70	–1.5 V vs. SCE	Carbon monoxide	70%	Magdesieva et al. [49]
	N-doped carbon nanofibers	0.5	–0.573 V vs. RHE	Carbon monoxide	98%	Kumar et al. [50]
	N-doped carbon fibers with a core of Ag nanowires	-	–0.8 V vs. RHE	Carbon monoxide Hydrogen	96%	Yang et al. [52]
	Au nanoparticles supported on graphene nanoribbon	~4–6	–0.47 V vs. RHE	Carbon monoxide	>60%	Rogers et al. [54]
Graphene	Cu ₂ O nanoparticles supported on graphene	-	–0.9 V vs. Ag/AgCl	Ethanol	9.93%	Geioushy et al. [55]
	N-doped graphene	7.5	–0.84 vs. Ag/AgCl	Formate	70–63%	Wang et al. [57]
	N-doped 3D-graphene foam	1.8	–0.58 V vs. RHE	Carbon monoxide Formic acid	70% 3.0%	Wu et al. [58]
	B-doped graphene	0.5	–1.4 V vs. SCE	Formate	66%	Sreekanth et al. [56]
	N-doped graphene	-	–0.9 V vs. RHE	Formate	65%	Li et al. [59]
	Cu nanoparticles dispersed on n-doped graphene		–0.9 V vs. RHE	Ethylene	19%	Li et al. [59]
	N-defective graphene	1.3	–0.6 V vs. RHE	Carbon monoxide	~84%	Han et al. [60]
Graphene Derivatives	Amine modified Au nanoparticles supported on rGO	6	–0.7 V vs. RHE	Carbon monoxide	>60%	Zhao et al. [64]
	Cu nanowires wrapped in rGO	8	–1.25 V vs. RHE	Methane	55%	Li et al. [65]
	Pt deposited on adenine-rGO	0.5	–0.3V vs. Ag/AgCl	Methanol	>85%	Hossein et al. [66]
	Cu ₂ O/N-doped rGO	12	–1.4 V vs. RHE	Ethylene	19.7%	Ning et al. [67]
	porphyrin/graphene framework	1.68	–0.54V vs. RHE	Carbon monoxide	98.7%	Choi et al. [69]
	Vitamin B6 grafted on GO sheet	0.25	–0.4 V vs. RHE	Ethanol	37%	Yuan et al. [70]
	iron porphyrin-based rGO hydrogel	0.42	–0.39 V vs. RHE	Carbon monoxide	96%	Choi et al. [72]
	Au nanoparticles supported on MWCNT	160	–1.78 V vs. Ag/AgCl	Carbon monoxide	60%	Jhong et al. [74]
	Au nanoparticles supported on MWCNT	158	–0.55 V vs. RHE	Carbon monoxide	85%	Verma et al. [75]
	SnOx supported on MWCNT	5–10	–1.4 V vs. SCE	Formic acid	60%	Zhao et al. [76]

Table 1. Cont.

Types of Carbon	Catalyst	Current Density (mA/cm ²)	Potential/Voltage	CO ₂ RR Products	Faradaic Efficiency	Reference
Supported Metal and Metal Derived Particles						
Carbon nanotubes	MWCNTs covered with a layer of Ag	350	−3 V cell voltage	Carbon monoxide	95%	Ma et al. [77]
	SnO ₂ /MWCNT with 20%weight of SnO ₂	80	−1.7 V vs. SCE	Formate	27.2%	Bashir et al. [78]
	Immobilized Mn complex in Nafion/MWCNT	2.65	−15 V vs. SCE	Carbon monoxide	24%	Walsh et al. [80]
	cobalt(II) chlorin complex	-	−1.1 V vs. NHE	Carbon monoxide	89%	Aoi et al. [82]
	Co phthalocyanine functionalised with CN groups anchored on CNT	15	−0.63 V vs. RHE −0.63 V vs. RHE	Carbon monoxide	>95%	Zhang et al. [84]
	CNT immobilized on cobalt polyphthalocyanine sheath	18.7	−0.5 V vs. RHE	Carbon monoxide	>80%	Han et al. [85]
	Co complex/CNT composite material	9.3	−0.48 V vs. RHE	Carbon monoxide	100%	Wang et al. [86]
	CNT embedded in a carbon matrix	6	−0.8 V vs. RHE	Formate	81%	Wang et al. [88]
	PEI-N-doped CNT	7.2	−1.8 V vs. SCE	Formate	85%	Zhang et al. [87]
	N-doped CNT	1	−0.8 V vs. RHE	Carbon monoxide	80%	Wu et al. [89]
Nitrogen-doped carbon nanotubes	N-doped CNT with pyridinic (1.1 at%) and graphitic (3.5 at%)	2	−1.05 V cell voltage (corrected for IR drop)	Carbon monoxide	80%	Sharma et al. [91]
	N-doped carbon wrapped CNT	0.5–0.1	−0.5 V vs. RHE	Carbon monoxide		Cui et al. [93]
	N-CNTs/SS	2	−1.1 V vs. Ag/AgCl	Carbon monoxide Hydrogen	75%	Liu et al. [94]

9. Conclusions and Future Prospects

In contrast with bulk carbon materials, the properties of carbon nanomaterials depend on a wide variety of parameters, such as structure, size, composition, orientation, defects, and fabrication method. The advances in nanotechnologies, for instance in nanocasting, electrodeposition, liquid-phase impregnation, chemical vapor deposition, and surfactant templating, allows unprecedented control over these parameters. This can lead to the development of new carbon materials with superior performances for a specific application. A continuous appearance of a multitude of new carbon materials obtained by combining different type of structures, by doping, functionalization, or their assembly into 3D nanostructures can be forecasted. In particular, modification of the surface chemistry of porous materials by chemical grafting, oxidation of the material surface, or by other means, will provide improved accessibility, a higher surface area and better dispersion of the active species for further improvement in their performance. Computational methods will play increasingly important roles in the understanding of reaction mechanisms and kinetics, in predicting new properties and in designing new materials. Coupling experiments with theoretical modeling surely will contribute to optimized customization of electrochemical properties of carbon materials for CO₂ER.

Among carbonaceous materials, carbon black as electrode constituent is the most studied, playing an important role in the several strategies for intensification of electrochemical CO₂ reduction.

In fact, noble metals nanoparticles supported on carbon black are the catalysts of the most advanced electrolyzers for gas-phase electro-reduction approaching a pilot demonstration phase [17,32,33]. Novel nanocarbon materials show in general modest results in terms of productivity. Low overpotentials are achieved at the expense of low current densities. However, it is evident, that these materials show the promise of surpassing the performance of state-of-the-art electrodes containing carbon black. This promise has already started to materialize in the work of Ma et al., whereby current densities higher than 300 mA cm^{-2} and energy efficiencies of 45% were achieved in a more optimized system [77]. This demonstrates that whole systems need to be studied and not only half cells, as well as the numerous parameters, which influence CO_2 electro-reduction, and in particular, electrolyser design must be optimized. Good catalysts are a key parameter for industrial deployment, but without the other process parameters being optimized they cannot show their full capabilities. Scale-up studies are needed posing interesting challenges to chemical engineers and chemists. Liquid phase electrolysis needs further breakthroughs in terms of materials for electrodes, membranes and electrolytes that will allow the higher mass transfer limitations to be overcome, when compared with gas-phase electrolysis. However, this operation mode presents important advantages namely allowing the integration of CO_2 capture and conversion [51] and achieving higher conversions avoiding the costs of separating unreacted CO_2 from gaseous electrolysis products [95,96]. The development of cost-effective 3D materials with pore engineered structures that can be used directly as electrodes is an important nascent R&D avenue. This strategy has the advantage of replacing state-of-the-art powder-based electrocatalysts. As previously mentioned, these catalysts are fabricated by mixing with electronically insulating polymer binders and pressing into pre-defined shapes. Although mature, these processes present the disadvantage of decreased overall cell electrical conductivity and contact between catalyst and electrolyte. This compromises the long-term performance and operation of electrolyzers. It is also difficult to reclaim the powders. This work shows that electro-catalysts based on nanocarbons are evolving towards more sophisticated architectures. However, one must keep an eye on the costs. The prices of the novel nanocarbons must be competitive with carbon black. This is not the current situation. Processes for graphene, carbon nanotubes etc. are more expensive and time consuming. This poses an enormous challenge to material scientists to develop scalable and cost-effective methods for the production of these products, turning them into competitive products.

Carbon black is derived from fossil fuels. The production of carbon materials from sustainable precursors, such as biomass and biochar from pyrolysis of sewage sludge for electrochemical CO_2 reduction, will be highly desirable as a low cost and sustainable approach.

Author Contributions: S.M. and A.S.R.-M. performed literature survey; Conceptualization and Writing-Original Draft Preparation, A.S.R.-M.; Visualization, S.M.; Editing, S.M.; A.S.R.-M.; M.N.d.P.; Review M.N.d.P.

Funding: This work was performed under the project “SunStorage—Harvesting and storage of solar energy”, with reference POCI-01-0145-FEDER-016387, funded by European Regional Development Fund (ERDF), through COMPETE 2020—Operational Programme for Competitiveness and Internationalisation (OPCI), and by national funds, through FCT—Fundação para a Ciência e a Tecnologia I.P.

Conflicts of Interest: The authors declare no conflicts of interest. The funders had no role in the design of the study; in the collection, analyses, or interpretation of data; in the writing of the manuscript, or in the decision to publish the results.

References

1. Kroto, H.W.; Heath, J.R.; O'Brien, S.C.; Curl, R.F.; Smalley, R.E. C_{60} : Buckminsterfullerene. *Nature* **1985**, *318*, 162–163. [[CrossRef](#)]
2. Iijima, S. Helical microtubules of graphitic carbon. *Nature* **1991**, *354*, 56–58. [[CrossRef](#)]
3. Kätelhön, A.; Meys, R.; Deutz, S.; Suh, S.; Bardow, A. Climate change mitigation potential of carbon capture and utilization in the chemical industry. *Proc. Natl. Acad. Sci. USA* **2019**, *116*, 11187–11194. [[CrossRef](#)]
4. Machado, A.S.R.; Nunes, A.V.M.; da Ponte, M.N. Carbon dioxide utilization—Electrochemical reduction to fuels and synthesis of polycarbonates. *J. Supercrit. Fluids* **2018**, *134*, 150–156. [[CrossRef](#)]
5. Dean, J.A. *Lange's Handbook of Chemistry*, 15th ed.; Mcgraw-Hill: New York, NY, USA, 1999; p. 1292.

6. Mahmood, M.N.; Masheder, D.; Harty, C.J. Use of gas-diffusion electrodes for high-rate electrochemical reduction of carbon dioxide. I. Reduction at lead, indium- and tin-impregnated electrodes. *J. Appl. Electrochem.* **1987**, *17*, 1159–1170. [[CrossRef](#)]
7. Hori, Y. Electrochemical CO₂ reduction on metal electrodes. In *Modern Aspects of Electrochemistry*; White, R.E., Gamboa-Aldeco, M.E., Vayenas, C.G., Eds.; Springer: New York, NY, USA, 2008; Volume 42, pp. 89–189.
8. Srinivasan, S. Experimental Methods in Low Temperature Fuel Cells. In *Fuel Cells from Fundamentals to Applications*; Springer: New York, NY, USA, 2006; pp. 268–306.
9. Mot, B.; Hereijgers, J.; Duarte, M.; Breugelmans, T. Influence of flow and pressure distribution inside a gas diffusion electrode on the performance of a flow-by CO₂ electrolyzer. *Chem. Eng. J.* **2019**, *378*. [[CrossRef](#)]
10. Furuya, N.; Yamazaki, T.; Shibata, M. High performance Ru-Pd catalysts for CO₂ reduction at gas diffusion electrodes. *J. Electroanal. Chem.* **1997**, *43*, 139–141. [[CrossRef](#)]
11. Cook, R.L.; Macduff, R.C.; Sammells, A.F. High rate CO₂ reduction to ethylene and methane using gas diffusion electrodes. *J. Electrochem. Soc.* **1990**, *137*, 607–608. [[CrossRef](#)]
12. Shibata, M.; Yoshida, K.; Furuya, N. Electrochemical Synthesis of Urea at Gas-Diffusion Electrodes. *J. Electrochem. Soc.* **1998**, *145*, 595–600. [[CrossRef](#)]
13. Hara, K.; Kudo, A.; Sakata, T.; Watanebe, M. High efficiency electrochemical reduction of carbon dioxide under high pressure on a gas diffusion electrode containing Pt catalysts. *J. Electrochem. Soc.* **1995**, *142*, L57–L59. [[CrossRef](#)]
14. Hara, K.; Sakata, T. Electrocatalytic Formation of CH₄ from CO₂ on a Pt Gas Diffusion Electrode. *J. Electrochem. Soc.* **1997**, *144*, 539–545. [[CrossRef](#)]
15. Hara, K.; Sakata, T. Large current density CO₂ reduction under high pressure using gas diffusion electrodes. *Bull. Chem. Soc. Jpn.* **1997**, *70*, 571–576. [[CrossRef](#)]
16. Zhao, G.; Jiang, T.; Han, B.; Li, Z.; Zhang, J.; Liu, Z.; He, J.; Wu, W. Electrochemical reduction of supercritical carbon dioxide in ionic liquid 1-n-butyl-3-methylimidazolium hexafluorophosphate. *J. Supercrit. Fluids* **2004**, *32*, 287–291. [[CrossRef](#)]
17. Dufek, E.J.; Lister, T.E.; Stone, S.G.; McIlwain, M.E. Operation of a Pressurized System for Continuous Reduction of CO₂. *J. Electrochem. Soc.* **2012**, *159*, F514–F517. [[CrossRef](#)]
18. Manthiram, K.; Beberwyck, B.J.; Alivisatos, A.P. Enhanced Electrochemical Methanation of Carbon Dioxide with a Dispersible Nanoscale Copper Catalyst. *J. Am. Chem. Soc.* **2014**, *136*, 13319–13325. [[CrossRef](#)]
19. Zhu, L.; Michalsky, R.; Metin, Ö.; Lv, H.F.; Guo, S.J.; Wright, C.J.; Sun, X.L.; Peterson, A.A.; Sun, S.H. Monodisperse Au Nanoparticles for Selective Electrocatalytic Reduction of CO₂ to CO. *J. Am. Chem. Soc.* **2013**, *135*, 16833–16836. [[CrossRef](#)]
20. Zhu, W.; Zhang, Y.J.; Zhang, H.; Lv, H.; Li, Q.; Michalsky, R.; Peterson, A.A.; Sun, S. Active and selective conversion of CO₂ to CO on ultrathin Au nanowires. *J. Am. Chem. Soc.* **2014**, *136*, 16132–16135. [[CrossRef](#)]
21. Douglas, R.; Kauffman, D.; Alfonso, C.; Matranga, H.F.; Qian, R.C.; Jin, R. Experimental and Computational Investigation of Au₂₅ Clusters and CO₂: A Unique Interaction and Enhanced Electrocatalytic Activity. *J. Am. Chem. Soc.* **2012**, *134*, 10237–10243.
22. Liu, S.; Tao, H.; Zeng, L.; Liu, Q.; Xu, Z.; Liu, Q.; Luo, J.L. Shape-dependent electrocatalytic reduction of CO₂ to CO on triangular silver nanoplates. *J. Am. Chem. Soc.* **2017**, *139*, 2160–2163. [[CrossRef](#)]
23. Kim, C.; Jeon, H.S.; Eom, T.; Jee, M.S.; Kim, H.; Friend, C.M.; Min, B.K.; Hwanga, Y.J. Achieving selective and efficient electrocatalytic activity for CO₂ reduction using immobilized silver nanoparticles. *J. Am. Chem. Soc.* **2015**, *137*, 13844–13850. [[CrossRef](#)]
24. Li, Q.; Fu, J.; Zhu, W.; Chen, Z.; Shen, B.; Wu, L.; Xi, Z.; Wang, T.; Lu, G.; Zhu, J.J.; et al. Tuning Sn-catalysis for electrochemical reduction of CO₂ to CO via the core/shell Cu/SnO₂ structure. *J. Am. Chem. Soc.* **2017**, *139*, 4290–4293. [[CrossRef](#)]
25. Azuma, M.; Hashimoto, K.; Hiramoto, M.; Watanabe, M.; Sakata, T. Electrochemical Reduction of Carbon Dioxide on Various Metal Electrodes in Low-Temperature Aqueous KHCO₃ Media. *J. Electrochem. Soc.* **1990**, *137*, 1772–1778. [[CrossRef](#)]
26. Noda, H.; Ikeda, S.; Oda, Y.; Imai, K.; Maeda, M.; Ito, K. Electrochemical reduction of carbon-dioxide at various metal-electrodes in aqueous potassium hydrogen carbonate solution. *Bull. Chem. Soc. Jpn.* **1990**, *63*, 2459–2462. [[CrossRef](#)]

27. Ohkawa, K.; Hashimoto, K.; Fujishima, A.; Noguchi, Y.; Nakayama, S. Electrochemical reduction of carbon dioxide on hydrogen storing materials: Part 1. The effect of hydrogen absorption on the electrochemical behavior on palladium electrodes. *Electroanal. Chem.* **1993**, *345*, 445–456. [[CrossRef](#)]
28. Hori, Y.; Wakebe, H.; Tsukamoto, T.; Koga, O. High Rate Gas Phase CO₂. Electrocatalytic process of CO selectivity in electrochemical reduction of CO₂ at metal electrodes in aqueous media. *Electrochim. Acta* **1994**, *39*, 1833–1839. [[CrossRef](#)]
29. Min, X.; Kanan, M.W. Pd-Catalyzed Electrohydrogenation of Carbon Dioxide to Formate: High Mass Activity at Low Overpotential and Identification of the Deactivation Pathway. *J. Am. Chem. Soc.* **2015**, *137*, 4701–4708. [[CrossRef](#)]
30. Del Castillo, A.; Alvarez-Guerra, M.; Solla-Gullón, J.; Sáez, A.; Montiel, V.; Irabien, A. Sn nanoparticles on gas diffusion electrodes: Synthesis, characterization and use for continuous CO₂ electroreduction to formate. *J. CO₂ Util.* **2017**, *18*, 222–228. [[CrossRef](#)]
31. Hou, P.; Wang, X.; Wang, Z.; Kang, P. Gas phase electrolysis of carbon dioxide to carbon monoxide using nickel nitride as the carbon enrichment catalyst. *ACS Appl. Mater. Interfaces* **2018**, *10*, 38024–38031. [[CrossRef](#)]
32. Kutz, R.; Chen, Q.; Yang, H.; Sajjad, S.D.; Liu, Z.; Masel, R.I. Sustainion imidazolium-functionalized polymers for carbon dioxide electrolysis. *Energy Technol.* **2017**, *5*, 929–936. [[CrossRef](#)]
33. Liu, Z.; Yang, H.; Kutz, R.; Masel, R.I. CO₂ Electrolysis to CO and O₂ at High Selectivity, Stability and Efficiency Using Sustainion Membranes. *J. Electrochem. Soc.* **2018**, *165*, J3371–J3377. [[CrossRef](#)]
34. Qiao, J.; Liu, Y.; Hong, F.; Zhang, J. A review of catalysts for the electroreduction of carbon dioxide to produce low-carbon fuels. *Chem. Soc. Rev.* **2014**, *43*, 631–675. [[CrossRef](#)] [[PubMed](#)]
35. Savinova, E.R.; Yashnik, S.A.; Savinov, E.N.; Parmon, V.N. Gas-phase electrocatalytic reduction of CO₂ to CO on carbon gas-diffusion electrode promoted by cobalt phthalocyanine. *React. Kinet. Catal. Lett.* **1992**, *46*, 249–254. [[CrossRef](#)]
36. Mahmood, M.N.; Masheded, D.; Harty, C.J. Use of gas-diffusion electrodes for high-rate electrochemical reduction of carbon dioxide. II. Reduction at metal phthalocyanine-impregnated electrodes. *J. Appl. Electrochem.* **1987**, *17*, 1223–1226. [[CrossRef](#)]
37. Shibata, M.; Furuya, N. Electrochemical synthesis of urea at gas-diffusion electrodes: Part VI. Simultaneous reduction of carbon dioxide and nitrite ions with various metallophthalocyanine catalysts. *J. Electroanal. Chem.* **2001**, *507*, 177–184. [[CrossRef](#)]
38. Shibata, M.; Furuya, N. Simultaneous reduction of carbon dioxide and nitrate ions at gas-diffusion electrodes with various metallophthalocyanine catalysts. *Electrochim. Acta* **2003**, *48*, 3953–3958. [[CrossRef](#)]
39. Wang, M.; Torbensen, K.; Salvatore, D.; Ren, S.; Joulié, D.; Dumoulin, F.; Mendoza, D.; Lassalle-Kaiser, B.; Isci, U.; Berlinguette, C.P.; et al. CO₂ electrochemical catalytic reduction with a highly active cobalt phthalocyanine. *Nat. Commun.* **2019**, *10*, 3602. [[CrossRef](#)]
40. Sonoyama, N.; Kirii, M.; Sakata, T. Electrochemical reduction of CO₂ at metal-porphyrin supported gas diffusion electrodes under high pressure CO₂. *Electrochem. Commun.* **1999**, *1*, 213–216. [[CrossRef](#)]
41. Castelo-Quibén, J.; Bailón-García, E.; Pérez-Fernández, F.J.; Carrasco-Marín, F.; Pérez-Cadenas, A.F. Mesoporous carbon nanospheres with improved conductivity for electro-catalytic reduction of O₂ and CO₂. *Carbon* **2019**, *155*, 88–99. [[CrossRef](#)]
42. Li, W.; Chen, D.; Li, Z.; Shi, Y.; Wan, Y.; Huang, J.; Yang, J.; Zhao, V.; Jiang, Z. Nitrogen enriched mesoporous carbon spheres obtained by a facile method and its application for electrochemical capacitor. *Electrochem. Commun.* **2007**, *9*, 569–573. [[CrossRef](#)]
43. Song, Y.; Chen, W.; Zhao, C.; Li, S.; Wei, W.; Sun, Y. Metal-Free Nitrogen-Doped Mesoporous Carbon for Electroreduction of CO₂ to Ethanol. *Angew. Chem. Int. Ed.* **2017**, *56*, 10840–10844. [[CrossRef](#)]
44. Kuang, M.; Guan, A.; Gu, Z.; Han, P.; Qian, L.; Zheng, G. Enhanced N-doping in mesoporous carbon for efficient electrocatalytic CO₂ conversion. *Nano Res.* **2019**, *12*, 2324–2329. [[CrossRef](#)]
45. Morlanés, N.; Takanabe, K.; Rodionov, V. Simultaneous reduction of CO₂ and splitting of H₂O by a single immobilized cobalt phthalocyanine electrocatalyst. *ACS Catal.* **2016**, *6*, 3092–3095. [[CrossRef](#)]
46. Rotundo, L.; Filippi, J.; Gobetto, R.; Miller, H.; Rocca, R.; Nervi, C.; Vizza, F. Electrochemical CO₂ reduction in water at carbon cloth electrodes functionalized with a fac-Mn(apbpy)(CO)₃Br complex. *Chem. Commun.* **2019**, *55*, 775–777. [[CrossRef](#)]
47. Coeuret, F.; Vilar, E.O.; Cavalcanti, E.B. Carbon fibre cloth as an electrode material: Electrical conductivity and mass transfer. *J. Appl. Electrochem.* **2002**, *32*, 1175–1182. [[CrossRef](#)]

48. Saito, N.; Aoki, K.; Usui, Y.; Shimizu, M.; Hara, K.; Narita, N.; Ogihara, N.; Nakamura, K.; Ishigaki, N.; Kato, H.; et al. Application of carbon fibers to biomaterials: A new era of nano-level control of carbon fibers after 30-years of development. *Chem. Soc. Rev.* **2011**, *40*, 3824–3834. [[CrossRef](#)] [[PubMed](#)]
49. Magdesieva, T.V.; Yamamoto, T.; Tryk, D.A.; Fujishima, A. Electrochemical Reduction of CO₂ with Transition Metal Phthalocyanine and Porphyrin Complexes Supported on Activated Carbon Fibers. *J. Electrochem. Soc.* **2002**, *146*, D89–D95. [[CrossRef](#)]
50. Kumar, B.; Asadi, M.; Pisasale, D.; Sinha-Ray, S.; Rosen, B.A.; Haasch, R.; Abiade, J.; Yarin, A.L.; Salehi-Khojin, A. Renewable and metal-free carbon nanofibre catalysts for carbon dioxide reduction. *Nat. Commun.* **2013**, *4*, 2819–2826. [[CrossRef](#)]
51. Reis-Machado, A.S.; Nunes da Ponte, M. CO₂ Capture and Electrochemical Conversion. *Curr. Opin. Green Sustain. Chem.* **2018**, *11*, 86–90. [[CrossRef](#)]
52. Yang, H.P.; Zhang, H.W.; Wu, Y.; Fan, L.D.; Chai, X.Y.; Zhang, Q.L.; Liu, J.H.; He, C.X. A core-shell-structured silver nanowire/nitrogen-doped carbon catalyst for enhanced and multifunctional electrofixation of CO₂. *ChemSusChem* **2018**, *11*, 3905–3910. [[CrossRef](#)]
53. Novoselov, K.S.; Geim, A.K.; Morozov, S.V.; Jiang, D.; Zhang, Y.S.V.; Grigorieva, V.; Firsov, A.A. Electric Field Effect in Atomically Thin Carbon Films. *Science* **2004**, *306*, 666–669. [[CrossRef](#)]
54. Rogers, C.; Perkins, W.S.; Veber, G.; Williams, T.E.; Cloke, R.R.; Fischer, F.R. Synergistic enhancement of electrocatalytic CO₂ reduction with gold nanoparticles embedded in functional graphene nanoribbon composite electrodes. *J. Am. Chem. Soc.* **2017**, *139*, 4052–4061. [[CrossRef](#)]
55. Geioushy, R.A.; Khaled, M.M.; Hakeem, A.S.; Khalid Alhooshani, K.; Basheer, C. High efficiency graphene/Cu₂O electrode for the electrochemical reduction of carbon dioxide to ethanol. *J. Electroanal. Chem.* **2017**, *785*, 138–143. [[CrossRef](#)]
56. Sreekanth, N.; Nazrulla, M.A.; Vineesh, T.V.; Sailaja, K.; Phani, K.L. Metal-free boron-doped graphene for selective electroreduction of carbon dioxide to formic acid/formate. *Chem. Commun.* **2015**, *51*, 16061–16064. [[CrossRef](#)] [[PubMed](#)]
57. Wang, H.X.; Chen, Y.B.; Hou, X.L.; Ma, C.Y.; Tan, T.W. Nitrogen-doped graphenes as efficient electrocatalysts for the selective reduction of carbon dioxide to formate in aqueous solution. *Green Chem.* **2016**, *18*, 3250–3256. [[CrossRef](#)]
58. Wu, J.J.; Liu, M.J.; Sharma, P.P.; Yadav, R.M.; Ma, L.L.; Yang, Y.C.; Zou, X.L.; Zhou, X.D.; Vajtai, R.; Yakobson, B.I.; et al. Incorporation of Nitrogen Defects for Efficient Reduction of CO₂ via Two-Electron Pathway on Three-Dimensional Graphene Foam. *Nano Lett.* **2016**, *16*, 466–470. [[CrossRef](#)] [[PubMed](#)]
59. Li, Q.; Zhu, W.; Fu, J.; Zhang, H.; Wu, G.; Sun, S. Controlled assembly of Cu nanoparticles on pyridinic-N rich graphene for electrochemical reduction of CO₂ to ethylene. *Nano Energy* **2016**, *24*, 1–9. [[CrossRef](#)]
60. Han, P.; Yu, X.M.; Yuan, D.; Kuang, M.; Wang, Y.F.; Al-Enizi, A.M.; Zheng, G.F. Defective graphene for electrocatalytic CO₂ reduction. *J. Colloid Interface Sci.* **2019**, *534*, 332–337. [[CrossRef](#)]
61. Chai, G.L.; Guo, Z.X. Highly effective sites and selectivity of nitrogen doped graphene/CNT catalysts for CO₂ electrochemical reduction. *Chem. Sci.* **2016**, *7*, 1268–1275. [[CrossRef](#)]
62. Reske, R.; Mistry, H.; Behafarid, F.; Cuenya, B.R.; Strasser, P. Particle Size Effects in the Catalytic Electroreduction of CO₂ on Cu Nanoparticles. *J. Am. Chem. Soc.* **2014**, *136*, 6978–6986. [[CrossRef](#)]
63. Mistry, H.; Reske, R.; Zeng, Z.H.; Zhao, J.; Greeley, J.; Strasser, P.; Cuenya, B.R. Exceptional Size-Dependent Activity Enhancement in the Electroreduction of CO₂ over Au Nanoparticles. *J. Am. Chem. Soc.* **2014**, *136*, 16473–16476. [[CrossRef](#)]
64. Zhao, Y.; Wang, C.; Liu, Y.; MacFarlane, D.R.; Wallace, G.G. Engineering Surface Amine Modifiers of Ultrasmall Gold Nanoparticles Supported on Reduced Graphene Oxide for Improved Electrochemical CO₂ Reduction. *Adv. Energy Mater.* **2018**, *8*. [[CrossRef](#)]
65. Li, Y.; Cui, F.; Ross, M.B.; Kim, D.; Sun, Y.; Yang, P. CO₂ electroreduction to hydrocarbons on ultrathin 5-fold twinned copper nanowires. *Nano Lett.* **2017**, *17*, 1312–1317. [[CrossRef](#)] [[PubMed](#)]
66. Alinajafi, H.A.; Ensafi, A.A.; Rezaei, B. Reduction of carbon dioxide to methanol on the surface of adenine functionalized reduced graphene oxide at a low potential. *Int. J. Hydrog. Energy* **2018**, *43*, 23262–23274.
67. Ning, H.; Mao, Q.; Wang, W.; Yang, Z.; Wang, X.; Zhao, Q.; Song, Y.; Wu, M. N-doped reduced graphene oxide supported Cu₂O nanocubes as high active catalyst for CO₂ electro-reduction to C₂H₄. *J. Alloy. Compd.* **2019**, *785*, 7–12. [[CrossRef](#)]

68. Zhou, X.; Micheroni, D.; Lin, Z.; Poon, C.; Li, Z.; Lin, W. Graphene-immobilized fac-Re(bipy)(CO)₃Cl for syngas generation from carbon dioxide. *ACS Appl. Mater. Interfaces* **2016**, *8*, 4192–4198. [[CrossRef](#)]
69. Choi, J.; Wagner, P.; Jalili, R.; Kim, J.; MacFarlane, D.R.; Wallace, G.G.; Officer, D.L. A porphyrin/graphene framework: A highly efficient and robust electrocatalyst for carbon dioxide reduction. *Adv. Energy Mater.* **2018**, *8*. [[CrossRef](#)]
70. Yuan, J.; Zhi, W.Y.; Liu, L.; Yang, M.P.; Wang, H.; Lu, J.X. Electrochemical reduction of CO₂ at metal-free N-functionalized graphene oxide electrodes. *Electrochim. Acta* **2018**, *282*, 694–701. [[CrossRef](#)]
71. Xu, Y.; Sheng, K.; Li, C.; Shi, G. Self-Assembled Graphene Hydrogel via a One-Step Hydrothermal Process. *ACS Nano* **2010**, *4*, 4324–4330. [[CrossRef](#)]
72. Choi, J.; Kim, J.; Wagner, P.; Gambhir, S.; Jalili, R.; Byun, S.; Sepidar, S.; Lee, Y.M.; MacFarlane, D.R.; Wallace, G.G.; et al. Energy efficient electrochemical reduction of CO₂ to CO using a three-dimensional porphyrin/graphene hydrogel. *Energy Environ. Sci.* **2019**, *12*, 747–755. [[CrossRef](#)]
73. Feng, X.; Kaili Jiang, K.; Fan, S.; Kanan, M.W. Grain-Boundary-Dependent CO₂ Electroreduction Activity. *J. Am. Chem. Soc.* **2015**, *137*, 4606–4609. [[CrossRef](#)]
74. Jhong, H.R.M.; Tornow, C.E.; Kim, C.; Verma, S.; Oberst, J.L.; Anderson, P.S.; Gewirth, A.A.; Fujigaya, T.; Nakashima, N.; Kenis, P.J.A. Gold Nanoparticles on Polymer-Wrapped Carbon Nanotubes: An Efficient and Selective Catalyst for the Electroreduction of CO₂. *ChemPhysChem* **2017**, *18*, 3274–3279. [[CrossRef](#)] [[PubMed](#)]
75. Verma, S.; Hamasaki, Y.; Kim, C.R.; Huang, W.; Lu, S.; Jhong, H.R.M.; Gewirth, A.A.; Fujigaya, T.; Nakashima, N.; Kenis, P.J.A. Insights into the low overpotential electroreduction of CO₂ to CO on a supported gold catalyst in an alkaline flow electrolyzer. *ACS Energy Lett.* **2018**, *3*, 193–198. [[CrossRef](#)]
76. Zhao, C.C.; Wang, J.L.; Goodenough, J.B. Comparison of electrocatalytic reduction of CO₂ to HCOOH with different tin oxides on carbon nanotubes. *Electrochem. Commun.* **2016**, *65*, 9–13. [[CrossRef](#)]
77. Ma, S.; Luo, R.; Gold, J.I.; Yu, A.Z.; Kim, B.; Kenis, P.J.A. Carbon nanotube containing Ag catalyst layers for efficient and selective reduction of carbon dioxide. *J. Mater. Chem. A* **2016**, *4*, 8573–8578. [[CrossRef](#)]
78. Bashir, S.; Hossain, S.S.; Rahmane, S.; Ahmed, S.; Al-Ahmed, A.; Hossain, M.M. Electrocatalytic reduction of carbon dioxide on SnO₂/MWCNT in aqueous electrolyte solution. *J. CO₂ Util.* **2016**, *16*, 346–353. [[CrossRef](#)]
79. Marepally, B.C.; Ampelli, C.; Genovese, C.; Tavella, F.; Veyre, L.; Quadrelli, E.A.; Perathoner, S.; Centi, G. Role of small Cu nanoparticles in the behaviour of nanocarbon-based electrodes for the electrocatalytic reduction of CO₂. *J. CO₂ Util.* **2017**, *21*, 534–542. [[CrossRef](#)]
80. Walsh, J.J.; Neri, G.; Smith, C.L.; Cowan, A.J. Electrocatalytic CO₂ reduction with a membrane supported manganese catalyst in aqueous solution. *Chem. Commun.* **2014**, *50*, 12698–12701. [[CrossRef](#)]
81. Walsh, J.J.; Smith, C.L.; Neri, G.; Whitehead, G.F.S.; Robertson, C.M.; Cowan, A.J. Improving the efficiency of electrochemical CO₂ reduction using immobilized manganese complexes. *Faraday Discuss.* **2015**, *183*, 147–160. [[CrossRef](#)]
82. Aoi, S.; Mase, K.; Ohkubo, K.; Fukuzumi, S. Selective electrochemical reduction of CO₂ to CO with a cobalt chlorin complex adsorbed on multi-walled carbon nanotubes in water. *Chem. Commun.* **2015**, *50*, 10226–10228. [[CrossRef](#)]
83. Hu, X.M.; Ronne, M.H.; Pedersen, S.U.; Skrydstrup, T.; Daasbjerg, K. Enhanced Catalytic Activity of Cobalt Porphyrin in CO₂. Electroreduction upon Immobilization on Carbon Materials. *Angew. Chem. Int. Ed.* **2017**, *56*, 6468–6472. [[CrossRef](#)]
84. Zhang, X.; Zishan Wu, Z.; Zhang, X.; Li, L.; Yanyan Li, Y.; Xu, H.; Li, X.; Xiaolu Yu, X.; Zhang, Z.; Liang, Y.; et al. Highly selective and active CO₂ reduction electrocatalysts based on cobalt phthalocyanine/carbon nanotube hybrid structures. *Nat. Commun.* **2017**, *8*, 14675–14682. [[CrossRef](#)] [[PubMed](#)]
85. Han, N.; Wang, Y.; Ma, L.; Wen, J.; Li, J.; Zheng, H.; Nie, K.; Wang, X.; Zhao, F.; Li, Y.; et al. Supported cobalt phthalocyanine for high-performance electrocatalytic CO₂ reduction. *Chem* **2017**, *3*, 652–664. [[CrossRef](#)]
86. Wang, M.; Chen, L.; Lau, T.-C.; Robert, M. Hybrid Co quaterpyridine complex/carbon nanotube catalytic material for CO₂ reduction in water. *Angew. Chem. Int. Ed.* **2018**, *57*, 7769–7773. [[CrossRef](#)] [[PubMed](#)]
87. Zhang, S.; Kang, P.; Ubnoske, S.; Brennaman, M.K.; Song, N.; House, R.L.; Glass, J.T.; Meyer, J. Polyethylenimine-enhanced electrocatalytic reduction of CO₂ to formate at nitrogen-doped carbon nanomaterials. *J. Am. Chem. Soc.* **2014**, *136*, 7845–7848. [[CrossRef](#)] [[PubMed](#)]

88. Wang, H.; Jia, J.; Song, P.; Wang, Q.; Li, D.; Min, S.; Qian, C.; Wang, L.; Li, Y.F.; Ma, C.; et al. Efficient Electrocatalytic Reduction of CO₂ by Nitrogen-Doped Nanoporous Carbon/Carbon Nanotube Membranes – A Step Towards the Electrochemical CO₂ Refinery. *Angew. Chem. Int. Ed.* **2017**, *56*, 7847–7852. [[CrossRef](#)]
89. Wu, J.J.; Yadav, R.M.; Liu, M.J.; Sharma, P.P.; Tiwary, C.S.; Ma, L.L.; Zou, X.L.; Zhou, X.D.; Yakobson, B.I.; Lou, J.; et al. Achieving Highly Efficient, Selective, and Stable CO₂ Reduction on Nitrogen-Doped Carbon Nanotubes. *ACS Nano* **2015**, *9*, 5364–5371. [[CrossRef](#)]
90. Sumpster, B.G.; Huang, J.; Meunier, V.; Romo-Herrera, J.M.; Cruz-Silva, E.; Terrones, H.; Terrones, M. A theoretical and experimental study on manipulating the structure and properties of carbon nanotubes using substitutional dopants. *Int. J. Quantum Chem.* **2009**, *109*, 97–118. [[CrossRef](#)]
91. Sharma, P.P.; Wu, J.J.; Yadav, R.M.; Liu, M.J.; Wright, C.J.; Tiwary, C.S.; Yakobson, B.I.; Lou, J.; Ajayan, P.M.; Zhou, X.D. Nitrogen-Doped Carbon Nanotube Arrays for High-Efficiency Electrochemical Reduction of CO₂: On the Understanding of Defects, Defect Density, and Selectivity. *Angew. Chem. Int. Ed.* **2015**, *54*, 13701–13705. [[CrossRef](#)]
92. Jiao, Y.; Zheng, Y.; Smith, S.C.; Du, A.J.; Zhu, Z.H. Electrocatalytically Switchable CO₂ Capture: First Principle Computational Exploration of Carbon Nanotubes with Pyridinic Nitrogen. *ChemSusChem* **2014**, *7*, 435–441. [[CrossRef](#)]
93. Cui, X.Q.; Pan, Z.Y.; Zhang, L.J.; Peng, H.S.; Zheng, G.F. Selective etching of nitrogen-doped carbon by steam for enhanced electrochemical CO₂ reduction. *Adv. Energy Mater.* **2017**, *7*, 1701456. [[CrossRef](#)]
94. Liu, K.H.; Zhong, H.X.; Yang, X.Y.; Bao, D.; Meng, F.L.; Yan, J.L.; Zhang, X.B. Composition-tunable synthesis of “clean” syngas via a one-step synthesis of metal-free pyridinic-N-enriched self-supported CNTs: The synergy of electrocatalyst pyrolysis temperature and potential. *Green Chem.* **2017**, *19*, 4284–4288. [[CrossRef](#)]
95. Diaz, L.A.; Gao, N.; Adhikari, B.; Lister, T.E.; Dufek, E.J.; Wilson, A.D. Electrochemical production of syngas from CO₂ captured in switchable polarity solvents. *Green Chem.* **2018**, *20*, 620–626. [[CrossRef](#)]
96. Messias, S.; Sousa, M.M.; Nunes da Ponte, M.; Rangel, C.M.; Pardal, T.; Reis-Machado, A.S. Electrochemical production of syngas from CO₂ at pressures up to 30 bar in electrolytes containing ionic liquid. *React. Chem. Eng.* **2019**, *4*, 1982–1990. [[CrossRef](#)]



© 2019 by the authors. Licensee MDPI, Basel, Switzerland. This article is an open access article distributed under the terms and conditions of the Creative Commons Attribution (CC BY) license (<http://creativecommons.org/licenses/by/4.0/>).